

BSM WW production with a jet veto

Luke Arpino,^a Andrea Banfi,^a Sebastian Jäger,^a Nikolas Kauer^b

^a*Department of Physics and Astronomy, University of Sussex, Brighton BN1 9QH, U.K.*

^b*Department of Physics, Royal Holloway, University of London, Egham Hill, Egham TW20 0EX, U.K.*

E-mail: l.arpino@sussex.ac.uk, a.banfi@sussex.ac.uk,
s.jaeger@sussex.ac.uk, n.kauer@rhul.ac.uk

ABSTRACT: We consider the impact on WW production of the unique dimension-six operator coupling gluons to the Higgs field. In order to study this process, we have to appropriately model the effect of a veto on additional jets. This requires the resummation of large logarithms of the ratio of the maximum jet transverse momentum and the invariant mass of the W boson pair. We have performed such resummation at the appropriate accuracy for the Standard Model (SM) background and for a signal beyond the SM (BSM), and devised a simple method to interface jet-veto resummations with fixed-order event generators. This resulted in the fast numerical code `MCFM-RE`, the Resummation Edition of the fixed-order code `MCFM`. We compared our resummed predictions with parton-shower event generators and assessed the size of effects, such as limited detector acceptances, hadronisation and the underlying event, that were not included in our resummation. We have then used the code to compare the sensitivity of WW and ZZ production at the HL-LHC to the considered higher-dimension operator. We have found that WW can provide complementary sensitivity with respect to ZZ , provided one is able to control theory uncertainties at the percent-level. Our method is general and can be applied to the production of any colour singlet, both within and beyond the SM.

Contents

1	Introduction	1
2	Gluon fusion (including BSM effects)	6
3	Quark-antiquark annihilation (SM only)	8
4	Numerical results	11
5	Sensitivity studies	21
6	Conclusions	28
A	Collection of relevant formulae	30
A.1	NLL resummation	31
A.2	NNLL resummation	32
A.3	Matching to fixed order and theoretical uncertainties	34
B	Numerical implementation in MCFM	36
B.1	Overview	36
B.2	Details of MCFM implementation	38

1 Introduction

Di-boson production at the Large Hadron Collider constitutes a promising window into physics beyond the SM. This is particularly true for di-boson pairs with high invariant mass, which have been already probed by a number of recent experimental analyses [1–11]. On the one hand, their production through gluon fusion receives contributions from an off-shell Higgs boson [12–14]. In particular, the interference of the contribution of an off-shell Higgs boson and di-boson continuum background makes it possible to access the Higgs width in a model-independent way [15]. On the other hand, contact interactions arising from higher-dimensional effective field theory operators [16–20] could give rise to spectacular effects in the tails of di-boson differential distributions, due to the fact that their contribution increases with energy. Technically, in the SM, di-boson production via gluon fusion is a loop-induced process. At low di-boson invariant masses, top quarks in the loops behave as very heavy particles, thus giving rise to effective contact interactions. At high invariant masses, the two bosons probe virtualities that are much larger than the masses of the

top quarks running in the loops, hence suppressing their contribution and enhancing the effect of BSM contact interactions. Such a feature has been already used to constrain the coefficient of a number of higher-dimensional operators, see e.g. [21] for a recent study.

In this article we restrict ourselves to considering the unique dimension-six operator coupling gluons to the Higgs boson, given by [17]

$$\mathcal{L} \supset \frac{c_{gg}}{\Lambda^2} G_{\mu\nu}^a G^{a,\mu\nu} \phi^\dagger \phi, \quad (1.1)$$

with $G_{\mu\nu}^a$ the gluon field strength and ϕ the Higgs field. This operator can be used to represent contributions to SM Higgs production from particles with mass of order $\Lambda \gg m_H$. This operator has previously been considered in high-invariant-mass ZZ production with a fully leptonic final state in [22, 23]. However, the leptonic final state for WW has larger cross section and so WW could give complementary or better sensitivity than leptonic final states for ZZ . However, in WW production, a tight jet veto is employed by experiments to suppress background from top-pair production. Such a veto “forbids” the radiation of jets from the initial-state partons, with the effect of suppressing not only the background, but also the operator-mediated signal. In the present case, the signal occurs through gluon fusion, whereas WW production is mainly driven by quark-antiquark annihilation. Since gluons radiate more than quarks, one expects the suppression due to a jet veto to be stronger for the signal than for the background. It is therefore important to address the general question of how BSM searches with WW production compare to ZZ in the presence of a jet veto.¹

The aim of this paper is to quantify in a simple way how the significance of such a BSM signal is affected by the presence of a jet veto. The same procedure can be applied to any BSM scenario that modifies the production rate of a colour singlet, for instance dimension-8 operators [32]. A similar study [33] investigates the impact of a jet veto in the determination of the Higgs width using interference. To be more specific, we veto all jets that have a transverse momentum (with respect to the beam axis) above $p_{t,\text{veto}}$. First we observe that, at the level of the matrix element squared, a generic BSM signal mediated by a single higher-dimensional operator consists of an interference piece and a quadratic piece:

$$|M_{\text{SM}}|^2 + 2\text{Re}(M_{\text{SM}}^* M_{\text{BSM}}) + |M_{\text{BSM}}|^2. \quad (1.2)$$

The last piece is of higher order $1/\Lambda^4$. Therefore, if the interference piece is not suppressed or vanishing for some reason, then, to a first approximation, we can neglect

¹In fact, a supposed discrepancy of the total WW cross section from SM predictions [24–26] could be partly ascribed to mismodelling of jet-veto effects [27–31].

it relative to the $1/\Lambda^2$ interference piece.² The presence of a jet veto induces large logarithms of the ratio of $p_{t,\text{veto}}$ and the invariant mass of the WW pair M_{WW} . Such logarithms arise at all orders in QCD, and originate from vetoing soft-collinear parton emissions. Considering just the leading logarithms, and neglecting the quadratic piece $|M_{\text{BSM}}|^2$, the deviation of a BSM signal that proceeds from gluon fusion from the SM prediction is approximately given by

$$\mathcal{L}_{gg}(M_{WW}) \times 2\text{Re}(M_{\text{SM}}^* M_{\text{BSM}}) e^{-2C_A \frac{\alpha_s}{\pi} \ln^2\left(\frac{M_{WW}}{p_{t,\text{veto}}}\right)}, \quad (1.3)$$

where $C_A = 3$, α_s is the strong coupling, and $\mathcal{L}_{gg}(M_{WW})$ is the gluon-gluon luminosity corresponding to a partonic centre-of-mass energy equal to M_{WW} . The effect of the jet veto is an exponential (Sudakov) suppression with respect to a naive Born-level estimate. Note also that, for fixed $p_{t,\text{veto}}$, such a suppression becomes more and more important, the higher the invariant mass of the WW pair. This is precisely where the contribution of the BSM operator in eq. (1.1) has the most impact on the signal. For the SM background, dominated by quark-antiquark annihilation, we have instead a contribution proportional to

$$\mathcal{L}_{q\bar{q}}(M_{WW}) \times |M_{\text{SM}}|^2 e^{-2C_F \frac{\alpha_s}{\pi} \ln^2\left(\frac{M_{WW}}{p_{t,\text{veto}}}\right)}, \quad (1.4)$$

with $C_F = 4/3$ and $\mathcal{L}_{q\bar{q}}(M_{WW})$ the quark-antiquark luminosity. The relative deviation from the SM can be obtained by integrating eqs. (1.3) and (1.4) over the appropriate phase space. Note that, for a fixed value of M_{WW} , the exponential encoding jet-veto effects factorise completely. Therefore, the relative deviation from the SM in the presence of the jet-veto is different from that obtained with a Born-level calculation by a factor

$$e^{-2(C_A - C_F) \frac{\alpha_s}{\pi} \ln^2\left(\frac{M_{WW}}{p_{t,\text{veto}}}\right)}. \quad (1.5)$$

For $\alpha_s = 0.1$, $M_{WW} = 1 \text{ TeV}$, $p_{t,\text{veto}} = 20 \text{ GeV}$, the above factor is about 0.2. Therefore, despite the gain in the number of events one has in WW production with respect to ZZ , the significance of the signal might be reduced due to jet-veto effects. This is why it is crucial to have an estimate of jet-veto effects that is as accurate as possible.

The first question we address is what accuracy we can aim for in the description of a BSM signal and a QCD background involving the production of a colour singlet. In the absence of large jet-veto corrections, a generic BSM signal can be predicted at Born-level, or leading order (LO), in QCD, whereas any QCD background is nowadays known at least at next-to-leading order (NLO). In the presence of a jet veto, the production of a system of invariant mass M is affected by logarithms of the ratio $p_{t,\text{veto}}/M$, which make fixed-order predictions unreliable. After the all-order

²Note that, if we consider more than one higher-dimensional operator, there are possibly other BSM effects of order $1/\Lambda^3$ or $1/\Lambda^4$ in the interference piece in general, which might still compete with or dominate over the quadratic piece.

resummation of $\ln(p_{t,\text{veto}}/M)$, the differential cross-section $d\sigma(p_{t,\text{veto}})/dM^2$ with no jets with a transverse momentum above $p_{t,\text{veto}}$ can be written in the form³

$$\frac{d\sigma(p_{t,\text{veto}})}{dM^2} = \frac{d\sigma_0}{dM^2} e^{Lg_1(\alpha_s L)} (G_2(\alpha_s L) + \alpha_s G_3(\alpha_s L) + \dots), \quad L \equiv \ln \frac{M}{p_{t,\text{veto}}}. \quad (1.6)$$

with $d\sigma_0/dM^2$ the corresponding LO cross section. The above expression is meaningful for $\alpha_s \ln(M/p_{t,\text{veto}}) \sim 1$ and misses terms that vanish as powers of $p_{t,\text{veto}}/M$ (possibly enhanced by logarithms). The leading logarithmic (LL) contributions exponentiate giving rise to the function $g_1(\alpha_s L)$, with α_s evaluated at a renormalisation scale of order M . Next-to-leading logarithmic terms (NLL) factorise from LL ones, and are embedded in the function $G_2(\alpha_s L)$. Next-to-next-to-leading logarithmic (NNLL) contributions, resummed by $G_3(\alpha_s L)$, are of relative order α_s with respect to NLL ones, and similarly one can define higher logarithmic accuracy. The knowledge of NLO correction to a QCD background process gives access to all ingredients to compute G_3 , i.e. to achieve NNLL accuracy, whereas the lack of knowledge of corrections of relative order α_s to a generic BSM process implies that the best accuracy one can aim at for such processes is NLL. Therefore, from the point of view of the accuracy of the resummation, having LO makes it possible to reach NLL accuracy, whereas NLO gives access to NNLL accuracy.

The most widely used method to estimate jet-veto effects are Monte Carlo event generators, which simulate the contribution of multiple soft-collinear QCD emissions. Although very flexible, these tools cannot formally guarantee more than LL accuracy, and at the moment require a considerable amount of tuning to reliably describe observables, like the cross section with a jet-veto in eq. (1.6), sensitive to QCD radiation from the initial state (see e.g. [35] for a recent study). In order to have more accurate predictions, one needs to consider analytical resummations.

Jet-veto effects in the production of a colour singlet have been computed at NNLL accuracy in QCD [36] and in soft-collinear effective theory (SCET) [37, 38].⁴ The calculation of [36] is implemented for Higgs and Z -boson production, inclusive in all decay products, in the program `JetVHeto` [39]. A NNLL resummation in SCET using the results of ref. [37] has been implemented in `amc@NLO` for the production of a generic colour singlet, fully exclusive in its decay products [29]. This implementation has been used to estimate jet-veto effects in WW production [29] in the SM, and for hypothetical Z' and W' bosons [40]. The specificity of this implementation is

³The general expression in eq. (1.6) holds because the transverse momentum of the leading jet has the property of recursive infrared and collinear (rIRC) safety [34].

⁴The resummed predictions of refs. [37, 38] include all constants multiplying the resummation at order α_s^2 , which are formally N³LL in the counting of eq. (1.6). However, the resummations of refs. [37, 38] do not account for all N³LL effects, and their accuracy is labelled NNLL'. The same accuracy can be obtained by matching a NNLL resummation with exact NNLO. Although feasible, this is beyond the scope of the present work.

the way it handles the so-called “beam functions”. These contain convolutions of appropriate coefficient functions with parton distributions, and are a general feature of NNLL resummations with hadrons in the initial state. In ref. [29], beam functions are precomputed and tabulated so as to replace traditional parton distribution functions. In this article, we discuss an alternative approach that implements the QCD resummation of ref. [36], fully exclusive in the decay products of the colour singlet, in a way that is not tied to a specific event generator (e.g. `aMC@NLO`), but that requires minimal and simple modifications of the setup that is already available in any NLO QCD program. The starting point is to observe that, in eq. (1.6), the factor multiplying leading logarithms is in fact a new perturbative series, whose coefficients are functions of $\alpha_s L$. As stated previously, NLL corrections have the same structure as Born-level contributions, while NNLL corrections closely resemble NLO contributions. Therefore, NLL resummation could just be obtained by an event-by-event reweighting of a Born-level generator by keeping only the functions g_1 and G_2 in eq. (1.6). This is enough to estimate jet-veto effects to the BSM production of a colour singlet. Including NNLL corrections, needed for a precise estimate of the corresponding SM background, is also possible in a general way. In fact, resummation effects originate from soft and/or collinear emissions in such a way that NNLL corrections share the same phase space with Born-level contributions, but are of relative order α_s . In all NLO calculations there is always a contribution that lives in the same phase space as the Born, and is of relative order α_s . This is the subtraction term that cancels the infrared singularities of virtual corrections. Therefore, to implement NNLL effects, we can just modify the appropriate subtraction term in the NLO event generator. Having done this, all other NNLL effects factorise, and can be accounted for by an event-by-event reweighting, so as to reproduce eq. (1.6). The whole procedure requires generating Born-level events only, and hence is much faster than a full NLO calculation. As will be clear later, the same approach can be used to interface resummations in SCET, provided one is able to rewrite results in terms of the functions G_2 and G_3 in eq. (1.6).

In the following two sections we give a detailed description of this procedure for the specific case of BSM effects induced by the operator in eq. (1.1). In section 2, we study the effect of such an operator on WW production with a jet veto. As discussed above, this operator induces a modification of the cross section of WW production through gluon fusion. We denote the (differential) cross section for gluon fusion, potentially including an additional BSM contribution, with $d\sigma_{gg}$. The main result of this section is a recipe to compute cross sections for WW production with a jet veto at NLL accuracy, fully exclusive in the decay products of the W bosons. In section 3 we compute the cross section for the dominant contribution to the SM background, which is WW production via quark-antiquark annihilation, again in the presence of a jet veto. We denote the cross-section for this process with $d\sigma_{q\bar{q}}$, and compute exclusive cross sections in the decay products of the W bosons, while

resumming $\ln(M_{WW}/p_{t,\text{veto}})$ at NNLL accuracy. The main result of this section is a general recipe to modify a NLO event generator for the production of any colour singlet so that it produces resummed cross-section with a jet veto at NNLL accuracy. In section 4 we present some numerical results for a simplified model derived from the Lagrangian in eq. (1.1), corresponding to a realistic experimental setup. We compare our resummed predictions with parton-shower event generators, and assess the size of effects, such as limited detector acceptances, hadronisation and the underlying event, that are not included in our resummation. In section 5 we perform some basic sensitivity studies to investigate the exclusion potential of the HL-LHC for the parameters of the simplified model of section 4. Finally, section 6 presents our conclusions.

2 Gluon fusion (including BSM effects)

Let us first consider WW production via gluon fusion, possibly with a modification of the amplitude induced by the BSM operator in eq. (1.1). For simplicity, we consider here the decays $WW \rightarrow e^+\nu_e\mu^-\bar{\nu}_\mu$ and $WW \rightarrow e^-\bar{\nu}_e\mu^+\nu_\mu$. As explained in the introduction, if we impose that all jets have a transverse momentum below a threshold value $p_{t,\text{veto}}$, the distribution in M_{WW}^2 , differential in the phase space of the leptons, is affected by the presence of large logarithms $\ln(M_{WW}/p_{t,\text{veto}})$, that have to be resummed to all orders to obtain sensible theoretical predictions. Specifically, we consider jets obtained by applying the anti- k_t algorithm [41] with a given radius R . At NLL accuracy, the best we can achieve for gluon fusion, the aforementioned observable is given by [36, 42]

$$\frac{d\sigma_{gg}^{\text{NLL}}(p_{t,\text{veto}})}{d\Phi_{\text{leptons}}dM_{WW}^2} = \mathcal{L}_{gg}^{(0)}(L, M_{WW}) e^{Lg_1(\alpha_s L) + g_2(\alpha_s L)}, \quad (2.1)$$

where $L = \ln(M_{WW}/p_{t,\text{veto}})$, $\alpha_s = \alpha_s(M_{WW})$, and explicit expressions for the functions $g_1(\alpha_s L)$ and $g_2(\alpha_s L)$ can be found, for instance, in ref. [36]. In particular, they are the same for any colour singlet that is produced via gluon fusion (e.g. Higgs production). Note that, at NLL accuracy, the resummed distribution in eq. (2.1) does not depend on the radius R of the jets [42].

The phase space of the leptons is given by

$$d\Phi_{\text{leptons}} = \frac{d^3\vec{p}_e}{(2\pi)^3 2E_e} \frac{d^3\vec{p}_{\nu_e}}{(2\pi)^3 2E_{\nu_e}} \frac{d^3\vec{p}_\mu}{(2\pi)^3 2E_\mu} \frac{d^3\vec{p}_{\nu_\mu}}{(2\pi)^3 2E_{\nu_\mu}} (2\pi)^4 \delta(p_e + p_\mu + p_{\nu_e} + p_{\nu_\mu} - p_1 - p_2), \quad (2.2)$$

with $p_\ell = (E_\ell, \vec{p}_\ell)$ is the four-momentum of lepton $\ell = e, \mu, \nu_e, \nu_\mu$, and $p_i = x_i P_i$, $i = 1, 2$ are the momenta of the incoming partons, carrying each a fraction x_i of the incoming proton momentum P_i .

Last, we have a process dependent “luminosity” factor $\mathcal{L}_{gg}^{(0)}$, given by⁵

$$\mathcal{L}_{gg}^{(0)}(L, M_{WW}) = \int dx_1 dx_2 |M_{\text{SM}}^{(gg)} + M_{\text{BSM}}^{(gg)}|^2 \delta(x_1 x_2 s - M_{WW}^2) \times \\ \times f_g(x_1, p_{t,\text{veto}}) f_g(x_2, p_{t,\text{veto}}). \quad (2.3)$$

The two main ingredients entering $\mathcal{L}_{gg}^{(0)}$ are:

- the SM amplitude $M_{\text{SM}}^{(gg)}$ for the production of a WW pair (and its decay products) through gluon fusion, which can be supplemented with an additional contribution $M_{\text{BSM}}^{(gg)}$ accounting for BSM effects;
- the gluon density in the proton $f_g(x, \mu_F)$ at the factorisation scale $\mu_F = p_{t,\text{veto}}$. This value of μ_F reflects the fact that the factorisation scale is the highest scale up to which the considered observable is inclusive with respect to multiple collinear emissions from the initial-state partons. Since all collinear emissions with a transverse momentum above $p_{t,\text{veto}}$ are vetoed, the factorisation scale has to be $p_{t,\text{veto}}$ (see e.g. [34] for a formal derivation).

By comparing eq. (2.1) to eq. (1.6), we obtain the function $G_2(\alpha_s L)$ resumming all NLL contributions:

$$G_2(\alpha_s L) = \frac{\mathcal{L}_{gg}^{(0)}(L, M_{WW})}{\mathcal{L}_{gg}^{(0)}(0, M_{WW})} e^{g_2(\alpha_s L)}. \quad (2.4)$$

So far, with the exception of ref. [29], such resummations have been obtained by devising process-dependent codes that produce numerical results for $\mathcal{L}_{gg}^{(0)}(L, M_{WW})$. For instance, the program `JetVHeto` [39] returns NNLL resummations integrated over the full phase space of the decay products of a Higgs or a Z boson. However, the luminosity in eq. (2.3) can be obtained by running any Born-level event generator. In fact, any such program will compute a Born-level cross-section in WW production via gluon fusion (possibly with BSM contributions) starting from the formula:

$$\frac{d\sigma_{gg}^{(0)}}{d\Phi_{\text{leptons}} dM_{WW}^2} = \int dx_1 dx_2 |M_{\text{SM}}^{(gg)} + M_{\text{BSM}}^{(gg)}|^2 \delta(x_1 x_2 s - M_{WW}^2) \times \\ \times f_g(x_1, \mu_F) f_g(x_2, \mu_F) = \mathcal{L}_{gg}^{(0)}(0, M_{WW}), \quad (2.5)$$

where μ_F here is the default factorisation scale in the considered Born-level generator. Therefore, to obtain the differential distribution in eq. (2.1), it is enough to set that factorisation scale μ_F to $p_{t,\text{veto}}$, and multiply the weight of each phase-space point

⁵Note that, since jet-veto measurements do not keep track of any correlation between the angle of the jet and the outgoing leptons, the logarithmically enhanced contributions due to the helicity of incoming gluons described in [43] are not present in our case, so eq. (2.3) is valid as is.

by $\exp[Lg_1(\alpha_s L) + g_2(\alpha_s L)]$. Note that, if the programs returns event files with information on M_{WW} for each event, or if one produces histograms binned in M_{WW} , the reweighting can be performed without any need to touch the Born-level generator code.

3 Quark-antiquark annihilation (SM only)

Since SM background processes are typically known at least to NLO, in the presence of a jet veto, the SM cross-section for WW production can be computed at NNLL accuracy. The corresponding NNLL resummed expression is given by

$$\frac{d\sigma_{q\bar{q}}^{\text{NNLL}}(p_{t,\text{veto}})}{d\Phi_{\text{leptons}}dM_{WW}^2} = \left(\mathcal{L}_{q\bar{q}}^{(0)}(L, M_{WW}) + \mathcal{L}_{q\bar{q}}^{(1)}(L, M_{WW}) \right) \times \\ \times (1 + \mathcal{F}_{\text{clust}}(R) + \mathcal{F}_{\text{correl}}(R)) \times e^{Lg_1(\alpha_s L) + g_2(\alpha_s L) + \frac{\alpha_s}{\pi} g_3(\alpha_s L)}, \quad (3.1)$$

where again $L = \ln(M_{WW}/p_{t,\text{veto}})$, $\alpha_s = \alpha_s(M_{WW})$, and $d\Phi_{\text{leptons}}$ is the lepton phase space defined in eq. (2.2). The functions g_1, g_2 and g_3 are reported in [36], and are the same as for Drell-Yan production. The dependence on the jet radius R appears for the first time at NNLL accuracy in the functions $\mathcal{F}_{\text{clust}}(R), \mathcal{F}_{\text{correl}}(R)$, whose explicit expressions can be found in [42].

At NNLL accuracy we have two process-dependent ‘‘luminosities’’ $\mathcal{L}_{q\bar{q}}^{(0)}$ and $\mathcal{L}_{q\bar{q}}^{(1)}$. The luminosity $\mathcal{L}_{q\bar{q}}^{(0)}$ is the analogue of $\mathcal{L}_{gg}^{(0)}$ of eq. (2.3), this time for a $q\bar{q}$ initiated process:

$$\mathcal{L}_{q\bar{q}}^{(0)}(L, M_{WW}) = \sum_{i,j} \int dx_1 dx_2 |M_{ij}^{(q\bar{q})}|^2 \delta(x_1 x_2 s - M_{WW}^2) f_i(x_1, p_{t,\text{veto}}) f_j(x_2, p_{t,\text{veto}}). \quad (3.2)$$

The only difference with respect to $\mathcal{L}_{gg}^{(0)}$ is the LO SM amplitude $M_{ij}^{(q\bar{q})}$, which is different from zero only if i, j is a quark-antiquark pair with the same flavour.

At NNLL accuracy we need to add the luminosity $\mathcal{L}_{q\bar{q}}^{(1)}$, which is of relative order α_s with respect to $\mathcal{L}_{q\bar{q}}^{(0)}$, and is given by

$$\mathcal{L}_{q\bar{q}}^{(1)}(L, M_{WW}) = \sum_{i,j} \int dx_1 dx_2 |M_{ij}^{(q\bar{q})}|^2 \delta(x_1 x_2 s - M_{WW}^2) \times \\ \times \left[f_i(x_1, p_{t,\text{veto}}) f_j(x_2, p_{t,\text{veto}}) \frac{\alpha_s(M_{WW})}{2\pi} \mathcal{H}^{(1)} + \right. \\ \left. \frac{\alpha_s(p_{t,\text{veto}})}{2\pi} \sum_k \left(\int_{x_1}^1 \frac{dz}{z} C_{ik}^{(1)}(z) f_k\left(\frac{x_1}{z}, p_{t,\text{veto}}\right) f_j(x_2, p_{t,\text{veto}}) + \{(x_1, i) \leftrightarrow (x_2, j)\} \right) \right]. \quad (3.4)$$

Here new ingredients appear:

- one-loop virtual corrections to WW production. They are included in the term $\mathcal{H}^{(1)}$, the coefficient of $\alpha_s(M_{WW})$;
- coefficient constants arising from real collinear radiation. They are included in the terms $C_{ik}^{(1)}(z)$, whose explicit expressions can be found in ref. [36], and are the same as for Drell-Yan production. They multiply $\alpha_s(p_{t,\text{veto}})$, which reflects the fact that the characteristic scale of collinear radiation in jet-veto cross sections is $p_{t,\text{veto}}$.

With reference to eq. (1.6), the function G_2 resumming NLL contributions is

$$G_2(\alpha_s L) = \frac{\mathcal{L}_{q\bar{q}}^{(0)}(L, M_{WW})}{\mathcal{L}_{q\bar{q}}^{(0)}(0, M_{WW})} e^{g_2(\alpha_s L)}, \quad (3.5)$$

whereas the function G_3 resumming NNLL contributions is

$$G_3(\alpha_s L) = \frac{e^{g_2(\alpha_s L)}}{\alpha_s \mathcal{L}_{q\bar{q}}^{(0)}(0, M_{WW})} \left[\mathcal{L}_{q\bar{q}}^{(1)}(L, M_{WW}) + \mathcal{L}_{q\bar{q}}^{(0)}(L, M_{WW}) \left(\mathcal{F}_{\text{clust}}(R) + \mathcal{F}_{\text{correl}}(R) + \frac{\alpha_s}{\pi} g_3(\alpha_s L) \right) \right]. \quad (3.6)$$

As explained in the previous section, the function $\mathcal{L}_{q\bar{q}}^{(0)}$ can be obtained from an appropriate Born-level program. The function $\mathcal{L}_{q\bar{q}}^{(1)}$ instead represents a correction to $\mathcal{L}_{q\bar{q}}^{(0)}$ of relative order α_s , that cannot be obtained from a LO calculation. A viable possibility to perform NNLL resummation would be to modify eq. (2.3) so that it includes the convolutions over the variable z in eq. (3.3), and implement the modification in a Born-level generator. This is the approach taken in ref. [29], and in some way underlying the current implementation of the `JetVHeto` program [39]. Here we want to present an alternative procedure. First, let us consider how the NLO WW cross section is calculated in a NLO event generator:

$$\frac{d\sigma_{q\bar{q}}^{\text{NLO}}(p_{t,\text{veto}})}{d\Phi_{\text{leptons}} dM_{WW}^2} = \frac{d\sigma_{q\bar{q}}^{(0)}}{d\Phi_{\text{leptons}} dM_{WW}^2} + \frac{d\sigma_{q\bar{q},v+ct}^{(1)}}{d\Phi_{\text{leptons}} dM_{WW}^2} + \frac{d\sigma_{q\bar{q},r}^{(1)}}{d\Phi_{\text{leptons}} dM_{WW}^2}. \quad (3.7)$$

The first term in the sum is the LO SM cross section $d\sigma_{q\bar{q}}^{(0)}/d\Phi_{\text{leptons}} dM_{WW}^2 = \mathcal{L}_{q\bar{q}}^{(0)}(0, M_{WW})$. The last term, $d\sigma_{q\bar{q},r}^{(1)}/d\Phi_{\text{leptons}} dM_{WW}^2$, represents NLO corrections coming from the emission of an extra parton. They include the counterterms needed to ensure their finiteness in four space-time dimensions. The second term, $d\sigma_{q\bar{q},v+ct}^{(1)}/d\Phi_{\text{leptons}} dM_{WW}^2$, gives NLO corrections arising from the sum of virtual corrections, and the counterterms integrated over the full extra-parton phase space. This contribution lives in the same phase-space as the Born contribution, and is of relative order α_s . It has the

form

$$\frac{d\sigma_{q\bar{q},v+ct}^{(1)}}{d\Phi_{\text{leptons}}dM_{WW}^2} = \frac{\alpha_s(\mu_R)}{2\pi} \sum_{i,j} \int dx_1 dx_2 |M_{ij}^{(q\bar{q})}|^2 \delta(x_1 x_2 s - M_{WW}^2) \left[f_i(x_1, \mu_F) f_j(x_2, \mu_F) \tilde{\mathcal{H}}^{(1)} + \sum_k \left(\int_{x_1}^1 \frac{dz}{z} \tilde{C}_{ik}^{(1)}(z) f_k\left(\frac{x_1}{z}, \mu_F\right) f_j(x_2, \mu_F) + \{(x_1, i) \leftrightarrow (x_2, j)\} \right) \right]. \quad (3.8)$$

In the above equation, μ_R, μ_F are the renormalisation and factorisation scales used by the NLO generator, $\tilde{\mathcal{H}}^{(1)}$ represents virtual corrections to $q\bar{q} \rightarrow WW$, and $\tilde{C}_{ik}^{(1)}(z)$ the integrated counterterms. The explicit expressions of $\tilde{\mathcal{H}}^{(1)}$ and $\tilde{C}_{ik}^{(1)}(z)$ depend on their actual implementation in the NLO generator, in particular on the employed subtraction scheme. However, the form of eq. (3.8) is the same as that of the NNLL luminosity $\mathcal{L}_{q\bar{q}}^{(1)}(L, M_{WW})$ in eq. (3.3). Therefore, by comparing eqs. (3.3) and (3.8), we find that $\mathcal{L}_{q\bar{q}}^{(1)}(L, M_{WW})$ can be implemented in a NLO event generator by performing the replacements

$$\begin{aligned} \frac{\alpha_s(\mu_R)}{2\pi} \tilde{\mathcal{H}}^{(1)} &\rightarrow \frac{\alpha_s(M_{WW})}{2\pi} \mathcal{H}^{(1)}, \\ \frac{\alpha_s(\mu_R)}{2\pi} \tilde{C}_{ik}^{(1)}(z) &\rightarrow \frac{\alpha_s(p_{t,\text{veto}})}{2\pi} C_{ik}^{(1)}(z), \end{aligned} \quad (3.9)$$

and by evaluating the parton distribution functions at the factorisation scale $\mu_F = p_{t,\text{veto}}$. Finally, in order to obtain the resummed distribution in eq. (3.1), we need to reweight each phase space point by

$$(1 + \mathcal{F}_{\text{clust}}(R) + \mathcal{F}_{\text{correl}}(R)) e^{Lg_1(\alpha_s L) + g_2(\alpha_s L) + \frac{\alpha_s}{\pi} g_3(\alpha_s L)}. \quad (3.10)$$

This rescaling can also be performed when constructing histograms, as long as one has access to M_{WW} for each bin, or for each event in an event record.

We have implemented this procedure in the code **MCFM-RE**,⁶ a suitable modification of the NLO program **MCFM** [44]. The actual implementation is richer than what has been discussed so far, because it allows a user to change the default renormalisation and factorisation scales, and contains additional features. Since these details are not relevant for a general discussion, we have omitted them here. The interested reader is referred to appendix A for the actual formulae we implement, and to appendix B for a short manual of the code.

In the following two sections, we use this implementation to produce numerical results and sensitivity studies for an explicit BSM model.

⁶Available on request.

4 Numerical results

Let us discuss first our results for WW production via $q\bar{q}$ annihilation. We consider W pairs produced at the LHC with $\sqrt{s} = 13$ TeV, specifically $W^+W^- \rightarrow e^+\nu_e\mu^-\bar{\nu}_\mu$ and $W^+W^- \rightarrow \mu^+\nu_\mu e^-\bar{\nu}_e$, and select the final state according to a simplified version of the experimental cuts of ref. [3], reported in table 1. Jets are reconstructed according to the anti- k_t algorithm [41] with a jet radius $R = 0.4$. In table 1 we encounter

Fiducial selection requirement	Cut value
p_T^ℓ	> 25 GeV
$ y_\ell $	< 2.5
$M_{e\mu}$	> 10 GeV
Number of jets with $p_T > 30$ GeV	0
$\cancel{E}_{T,\text{Rel}}$	> 15 GeV
\cancel{E}_T	> 20 GeV

Table 1. Definition of the $WW \rightarrow e\mu$ fiducial phase space, where p_T^ℓ, y_ℓ are the transverse momentum and rapidity of either an electron or a muon, $M_{e\mu}$ is the invariant mass of the electron-muon pair, \cancel{E}_T is the missing transverse energy, and $\cancel{E}_{T,\text{Rel}}$ is defined in eq. (4.1).

the newly introduced observable $\cancel{E}_{T,\text{Rel}}$, which is defined as follows [45]:

$$\cancel{E}_{T,\text{Rel}} = \begin{cases} \cancel{E}_T \sin \Delta\phi, & \text{if } \Delta\phi \leq \frac{\pi}{2} \\ \cancel{E}_T, & \text{if } \Delta\phi > \frac{\pi}{2} \end{cases} \quad (4.1)$$

with $\Delta\phi = \min(|\phi_e - \phi_{\text{MET}}|, |\phi_\mu - \phi_{\text{MET}}|)$, and ϕ_e, ϕ_μ and ϕ_{MET} the azimuthal angle of the electron, the muon and the missing transverse energy respectively.

In our analysis, we omit b quark-initiated contributions to $pp \rightarrow WW$. At LO, the $b\bar{b}$ scattering subprocess contributes only 1% to the cross section. The gb and $g\bar{b}$ subprocesses, which enter at NLO QCD increase the NLO cross section by a factor 1.5. This large increase is due to graphs like $gb \rightarrow W^-(t \rightarrow W^+b)$. Such graphs feature a resonant top quark propagator, which effects an enhancement of $\mathcal{O}(m_t/\Gamma_t) = \mathcal{O}(10^2)$, which compensates the $\mathcal{O}(1\%)$ suppression due to the b PDF, and altogether an $\mathcal{O}(1)$ contribution is obtained. This contribution is commonly attributed to Wt production and decay (at LO QCD) [46], and hence has to be omitted in the NLO QCD corrections to WW production, which we consider here.

We now produce both NLO, NNLL resummed, and matched NLO+NNLL (with the matching procedure explained in appendix A.3) predictions for the differential distribution $d\sigma/dM_{WW}$ using PDF4LHC15 parton distribution functions (PDFs) at NLO [47], accessed through LHAPDF6 [48], corresponding to $\alpha_s(M_Z) = 0.118$, and we set both renormalisation and factorisation scales at $M_{WW}/2$, as customary in Higgs

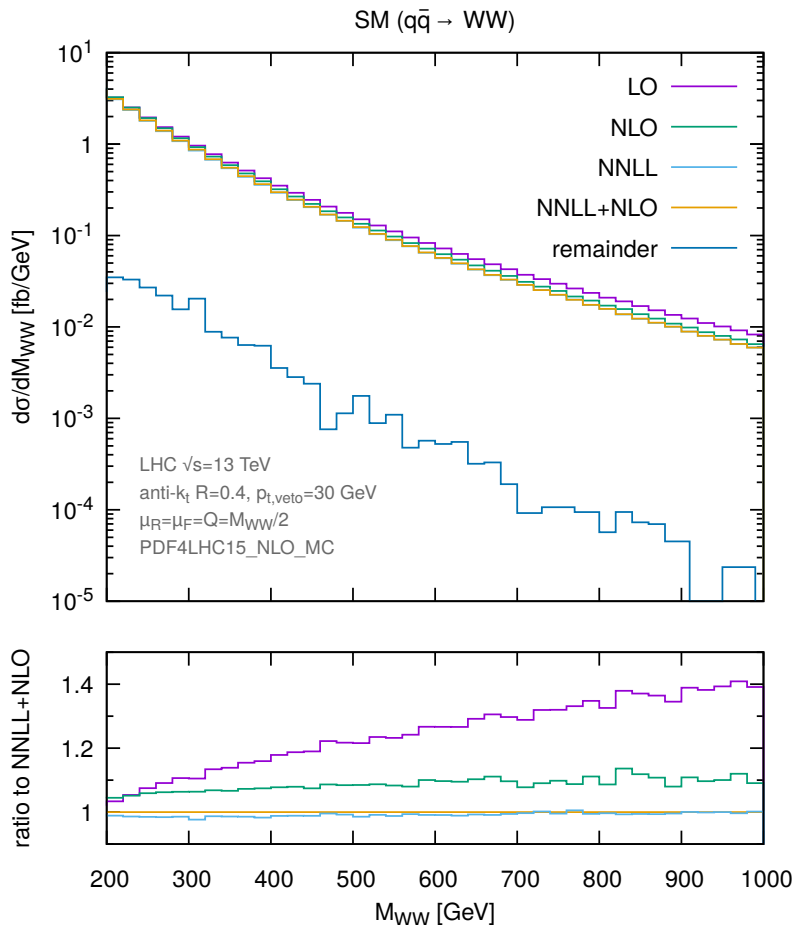


Figure 1. The differential distribution $d\sigma/dM_{WW}$ in the Standard Model, computed at different accuracies, and for the cuts described in the main text.

precision studies [49]. Fig. 1 shows the differential cross section in the invariant mass M_{WW} of the WW pair. We first note that both NLO and NNLL+NLO are both smaller than the LO, as expected due to the presence of a jet veto, with the suppression with respect to LO increasing with M_{WW} . This implies that, in this situation, a naive Born-level calculation fails to capture this effect and that, in the absence of a resummation, one should use at least a NLO prediction. NNLL+NLO gives a mild extra suppression with respect to NLO, revealing that logarithms are not particularly large in the considered kinematical region. However, we note that the difference between pure NNLL resummed and matched NNLL+NLO (the so-called “remainder”), which contains the part of the NLO which is not enhanced by logarithms, is basically negligible. This means that the resummation alone is very close to the best prediction we have at this order. This is remarkable in view of the fact that to obtain NNLL predictions we need to perform a calculation with Born-

level kinematics. On the contrary, the computational cost of the NLO calculation is larger due to the presence of an extra emission, without any significant gain in accuracy compared to the NNLL prediction.

To complete our discussion of the $q\bar{q}$ channel, we compare our predictions to those obtained from SCET via the program `aMC@NLO-SCET` of ref. [29]. The comparison is shown in Fig. 2. Our results contains theoretical uncertainties evaluated both

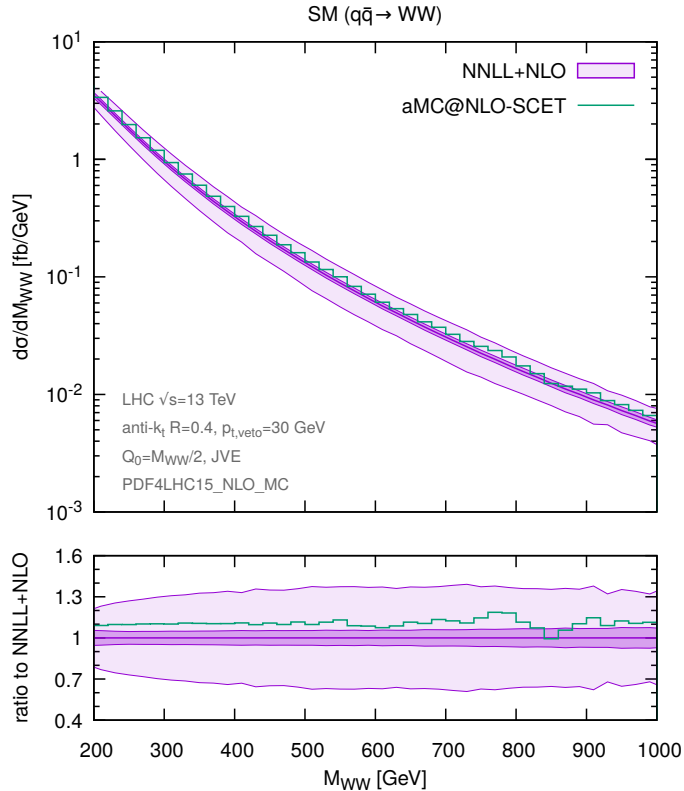


Figure 2. The differential distribution $d\sigma/dM_{WW}$ in the Standard Model, computed with our method, and with the program `aMC@NLO-SCET` [29]. See the main text for details.

with the most recent jet-veto efficiency (JVE) method [50] at the relevant accuracy (the wider, lighter band), and pure scale variations (the tighter, darker band). The details of both prescriptions can be found in appendix A. The SCET prediction corresponds to the default scale choices, and is well within JVE uncertainties, but slightly outside the boundary of scale variation uncertainties. Note that the most recent JVE prescription [50] requires the so-called “resummation scale” (the scale up to which soft-collinear resummations are assumed to be valid) to be varied by a factor of 1.5 rather than the factor of 2 used to vary renormalisation and factorisation scales (see appendix A for details). We have checked that also varying the resummation scale by a factor of 2 does not significantly increase the scale-uncertainty band, and the central prediction of [29] still lies outside that band. We remark that we do

not expect perfect agreement, because, although our methods and that of [29] share the same formal accuracy, they differ in the treatment of subleading effects. Our analysis suggests that scale uncertainties are not sufficient to capture the size of the neglected effects, and that other methods, such as the JVE or the one of [51], should be employed to have a more realistic estimate of theoretical uncertainties. A last comment is in order here. Within MCFM, we do not have access to NNLO calculations for di-boson production, so we cannot match our resummed predictions to NNLO. As a result of this, the JVE method may be overly conservative, due to the largish (~ 1.5) K-factor of the WW inclusive total cross-section, which propagates in the evaluation of the uncertainty according to the JVE method. If we could match to NNLO, the JVE uncertainty would be reduced and, as happens for Higgs production [36], would probably get closer to plain scale uncertainties.

In order to have a specific example of a BSM theory that implements the effective operator of eq. (1.1), we consider the following modification of the SM Lagrangian [52]:

$$\mathcal{L} \supset -\kappa_t \frac{m_t}{v} h \bar{t} t + \kappa_g \frac{\alpha_s}{12\pi} \frac{h}{v} G_{\mu\nu}^a G_a^{\mu\nu}, \quad (4.2)$$

with t , h , $G_{\mu\nu}^a$ the top field, the SM Higgs field, and the gluon field strength respectively. The SM corresponds to $(\kappa_t, \kappa_g) = (1, 0)$, and in this section we will only explore BSM scenarios such that $\kappa_t + \kappa_g = 1$, which ensures that the Higgs total cross section stays unchanged (modulo quark-mass effects, which give a correction of a few percent [50]). Such modifications of the SM Lagrangian only affect the gluon-fusion contribution to di-boson production. Their effect has been investigated before for the case of ZZ production [23], where one does not need to impose a jet veto to suppress unwanted background. Here we wish to study how the presence of a jet veto, required for studies of WW production, affects the relative size of a BSM contribution with respect to the SM background. We consider the three benchmark scenarios studied in ref. [23], i.e.

$$(\kappa_t, \kappa_g)_{\text{SM}} = (1, 0), \quad (\kappa_t, \kappa_g)_{\text{BSM}_1} = (0.7, 0.3), \quad (\kappa_t, \kappa_g)_{\text{BSM}_2} = (0, 1). \quad (4.3)$$

First, in Fig. 3 we compare the loop-induced gluon fusion contribution to the M_{WW} distribution at LO, which is what is given by default by any automated Born-level event generator, with the NLL analytic resummation, which gives the best modelling of jet-veto effects at the currently available accuracy. Our best $q\bar{q}$ prediction is also shown for comparison. We see that, if we include resummation effects, the cross section for each benchmark point is reduced by almost an order of magnitude in the tail of the distribution, where BSM effects start to become important. We then investigate more quantitatively how this impacts the deviations we might observe with respect to the SM, by plotting the quantity

$$\delta(M_{WW}) = \frac{d\sigma_{gg}^{\text{BSM}}/dM_{WW} - d\sigma_{gg}^{\text{SM}}/dM_{WW}}{d\sigma_{q\bar{q}}/dM_{WW}}. \quad (4.4)$$

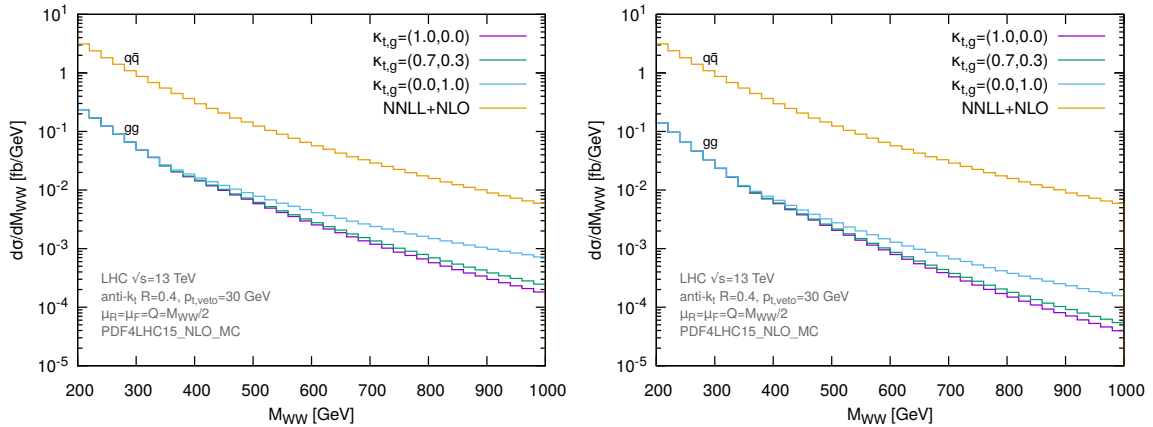


Figure 3. The differential cross section $d\sigma/dM_{WW}$ for the three benchmark scenarios of eq. (4.3), at LO (left) and at NLL (right) accuracy.

In the above equation, $d\sigma_{gg}^{\text{BSM}}$ is computed according to eq. (2.1), $d\sigma_{gg}^{\text{SM}}$ differs from $d\sigma_{gg}^{\text{BSM}}$ by the fact that the BSM contribution to the amplitude (M_{gg}^{BSM} in eq. (2.3)) is set to zero, and $d\sigma_{q\bar{q}}$ follows from eq. (3.1). Fig. 4 (left) shows $\delta(M_{WW})$ for the benchmark point (0.7, 0.3). We first note the growth of this quantity with energy, as expected from the effective nature of the ggH vertex. Fortunately, the growth persists after including jet-veto effects through NLL resummation, however the deviation from the SM reduces from the 1% that one would obtain using fixed-order calculations (see fig. 3) to fractions of a percent. The same quantity shown in the right panel of fig. 4 for the benchmark point (0.0, 1.0) displays qualitatively the same behaviour, although the deviation is a factor ten bigger. We see that, in the presence of jet-veto restrictions such as the one in ATLAS cuts [3], one is bound to use a theoretical tool that resums large logarithms. This could be either resummed predictions, or simulations with parton-shower event generators.

The variable $\delta(M_{WW})$ is of theoretical interest only, because we do not have access to the momenta of the neutrinos. To have experimentally accessible observables, we consider differential distributions in M_{T1} [53], M_{T2} [54] and M_{T3} [53], three measurable variables that are strongly correlated with M_{WW}

$$M_{T1} = \sqrt{(M_{T,e\mu} + \not{p}_T)^2 - (\vec{p}_{T,e\mu} + \vec{\not{p}}_T)^2}, \quad M_{T,e\mu} = \sqrt{p_{T,e\mu}^2 + M_{e\mu}^2}, \quad (4.5a)$$

$$M_{T2} = \sqrt{2p_{T,e\mu}\not{p}_T(1 - \cos \Delta\phi_{e\mu,\text{miss}})}, \quad (4.5b)$$

$$M_{T3} = \sqrt{(M_{T,e\mu} + M_T)^2 - (\vec{p}_{T,e\mu} + \vec{\not{p}}_T)^2}, \quad M_T = \sqrt{\not{p}_T^2 + M_{e\mu}^2}. \quad (4.5c)$$

In the above equations, $\vec{p}_{T,e\mu} = \vec{p}_{T,e} + \vec{p}_{T,\mu}$, and $M_{e\mu}^2 = (p_e + p_\mu)^2$. The vector $\vec{\not{p}}_T$ is the missing transverse momentum, defined as minus the vector sum of all detectable particles. Note that, if no jets are present, as at Born-level and in NNLL resummed

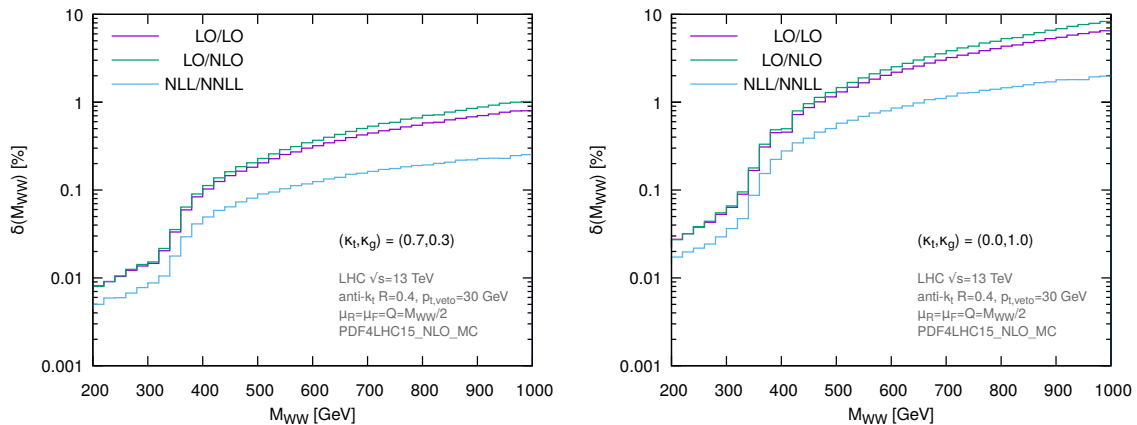


Figure 4. The relative difference between BSM and SM $d\sigma/dM_{WW}$ defined in eq. (4.4) for the two benchmark scenarios $(\kappa_t, \kappa_g)_{\text{BSM}_1}$ (left) and $(\kappa_t, \kappa_g)_{\text{BSM}_2}$ (right). The labels refer to the accuracy employed in the calculation of numerator and denominator in eq. (4.4).

predictions, $\vec{p}_T = -\vec{p}_{T,e\mu}$. Last, $\Delta\phi_{e\mu,\text{miss}}$ is the azimuthal angle between $\vec{p}_{T,e\mu}$ and \vec{p}_T . The corresponding results for δ are shown in Fig. 5. We note that M_{T2} gives rise

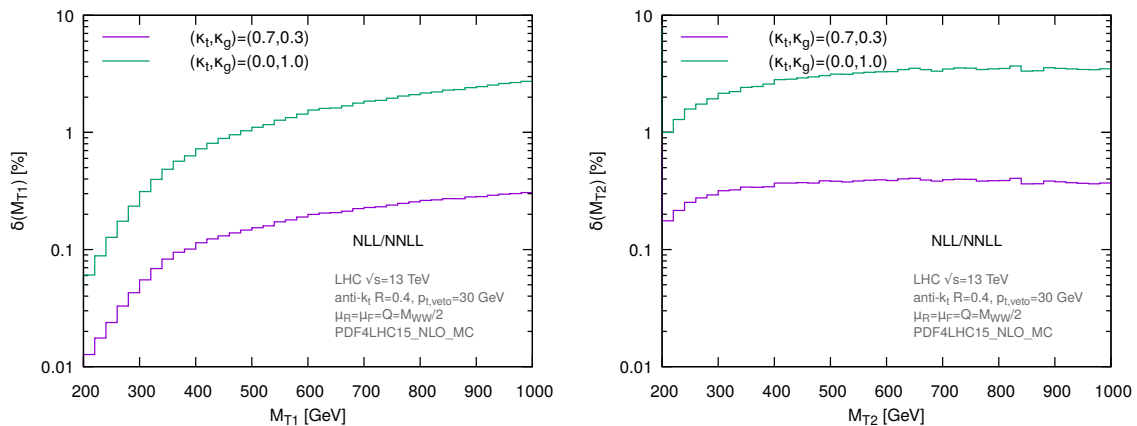


Figure 5. The relative difference between BSM and Standard Model WW production, differential in M_{T1} (left) and M_{T2} (right).

to considerably larger deviations with respect to M_{T1} . This is because low values of M_{T2} are correlated to larger values of M_{WW} , so M_{T2} effectively probes the M_{WW} distribution in the high-mass tail, where BSM effects are appreciable. However, this also means that the differential cross section in M_{T2} is much smaller than that in M_{T1} , as can be seen from Fig. 6. Therefore, the discriminatory power of M_{T2} is only of use if we have a very large number of events. We have also studied the variable M_{T3} defined again in ref. [54] and first devised in ref. [55]. The distribution in this variable looks very similar to that of $2M_{T1}$, so the same discussion as for M_{T1} applies here.

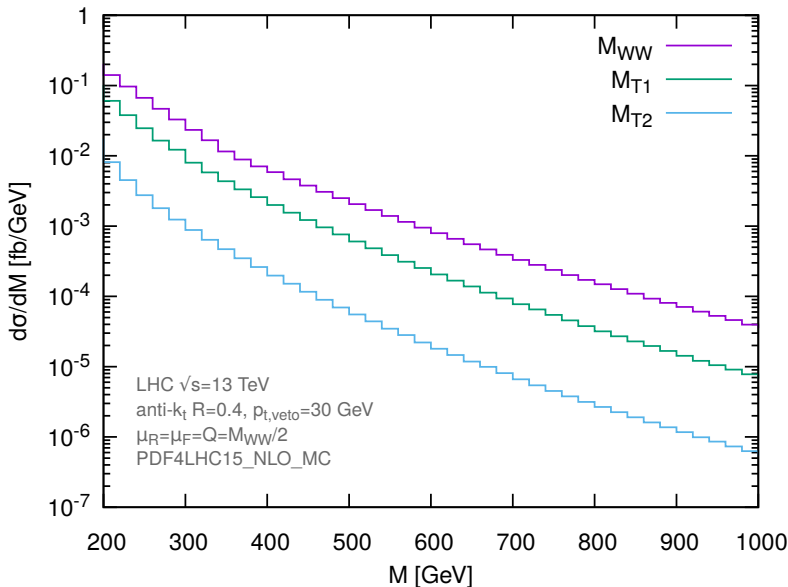


Figure 6. The distributions in $M = M_{WW}, M_{T1}, M_{T2}$ for the gg incoming channel.

We now compare our results to parton-level predictions from parton-shower event generators, using existing tunes. In particular, for $q\bar{q}$ we consider POWHEG [56–59] matched to the AZNLO [35] tune of PYTHIA v8.230 [60], and aMC@NLO [61–65] matched to PYTHIA, this time with the default parameters. To investigate the dependence on the shower algorithm, we also consider the parton shower HERWIG v7.1.0 [66, 67] matched as POWHEG+HERWIG, and aMC@NLO+HERWIG, both with the default parameters. For POWHEG+PYTHIA, we use the PDF set by the AZNLO tune, i.e. CT10 [68] for POWHEG and CTEQ6L1 [69] for the parton shower. For consistency, we use CT10 everywhere for POWHEG+HERWIG. For POWHEG+HERWIG, we also performed runs with default shower PDFs, and noted no significance difference in the resulting distributions. For all the aMC@NLO runs we use PDF4LHC15 PDFs, both for the generation of the hard configurations and the shower.

The comparison of resummation with event generators is shown in Fig. 7 for the SM (for $q\bar{q} \rightarrow WW$ and $gg \rightarrow WW$ separately), and in Fig. 8 for the two BSM scenarios considered above. Resummed predictions include an estimate of theory uncertainties at the appropriate accuracy, as explained in appendix A.3. Note that, due to the missing NLO total cross-section for the incoming gg channel, JVE and scale uncertainties for $gg \rightarrow WW$ are of comparable size, with the JVE ones slightly larger. We first observe that, both for $q\bar{q}$ - and for gg -initiated WW production, all event generators agree with the resummation within its uncertainties. For $q\bar{q}$, where we can match parton-shower predictions to NLO, POWHEG+PYTHIA shows a remarkable agreement with the resummation, but other event generators give comparable results. We note that predictions obtained with aMC@NLO show a slightly different trend with

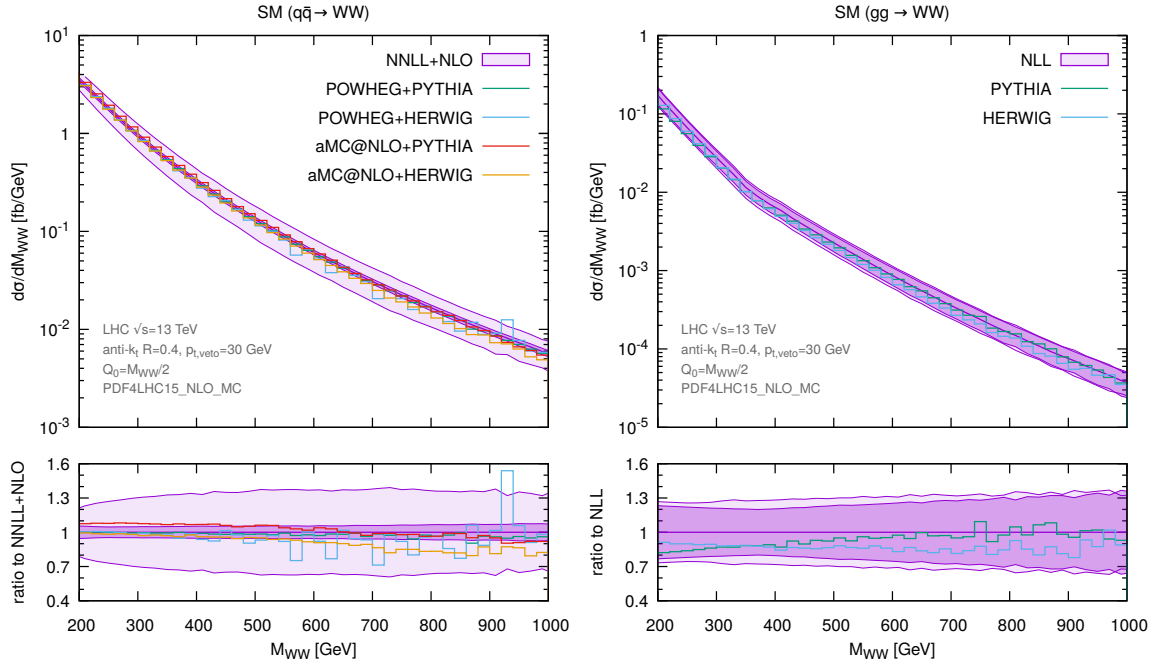


Figure 7. Analytical predictions for the SM distribution in the invariant mass of a WW pair, compared to results from various parton-shower event generators, corresponding to the details given in the main text.

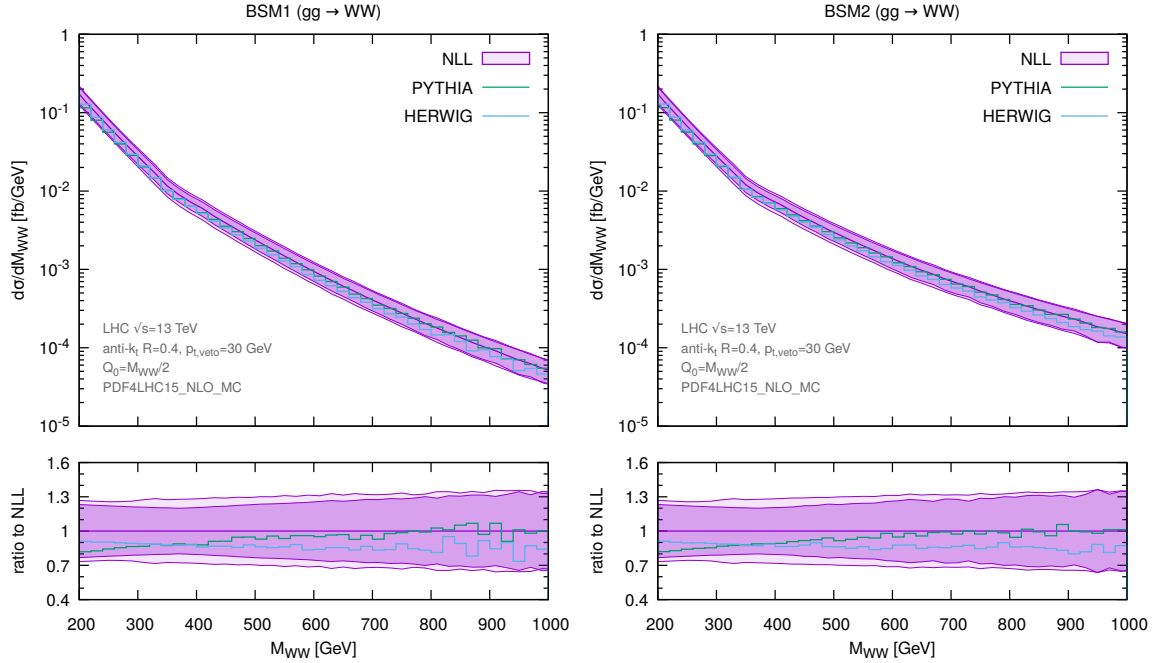


Figure 8. The same distribution as in Fig. 7 for the two BSM scenarios considered in the main text.

M_{WW} . In particular aMC@NLO+PYTHIA is slightly above our central prediction at low M_{WW} , and a bit lower at high M_{WW} , whereas aMC@NLO+HERWIG shows the same trend but is everywhere lower than our predictions.

In the gg case, both for the SM and the considered BSM scenarios, we can only compare to unmatched parton-showers results, as no NLO calculation is available. We observe that PYTHIA is in better agreement with our predictions at large values of M_{WW} , whereas HERWIG's predictions have the same shape as ours, but are systematically lower by about 10%. Overall, there is agreement between our predictions and parton showers within uncertainty bands, so the latter can be reliably used for this process. We remark that parton-shower predictions not only have lower formal accuracy, but are also much more expensive computationally. Hence it might be lengthy to assess with those tools if a range of BSM parameters leads to sizeable deviations from the SM, whereas with our numerical implementation such analyses could be performed at the cost of an unshowered Born-level calculation.

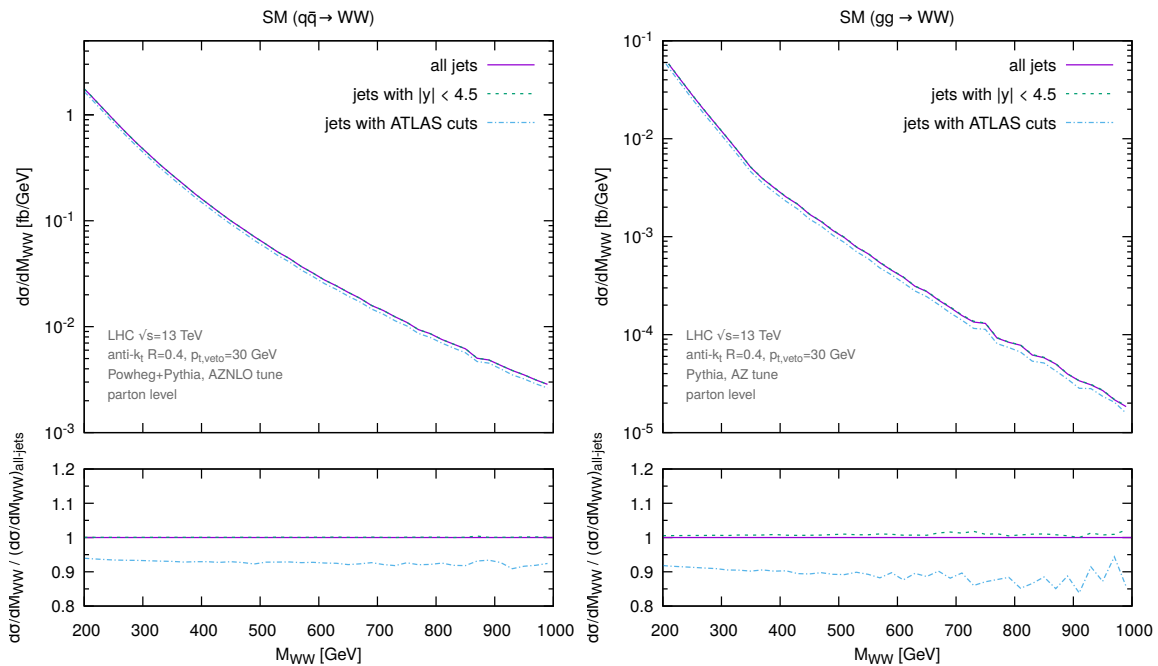


Figure 9. Impact of different cuts on the jets on $d\sigma/dM_{WW}$ in the SM for $q\bar{q}$ (left) modelled with POWHEG+PYTHIA and gg (right) modelled with plain PYTHIA.

We now investigate the impact of actual ATLAS cuts on the jets with respect to the simplified cuts in table 1. First, ATLAS vetoes only jets with $|y| < 4.5$. This might cause problems for our resummed calculation because, according to the argument of ref. [70], it limits its validity to $\ln(M_{WW}/p_{t,\text{veto}}) \lesssim 4.5$. Also, ATLAS employs an additional cut on the jets, vetoing also jets with $p_T > 25$ GeV and $|y| < 2.5$. If we compute $d\sigma/dM_{WW}$ with the cuts in table 1, we miss a contribution

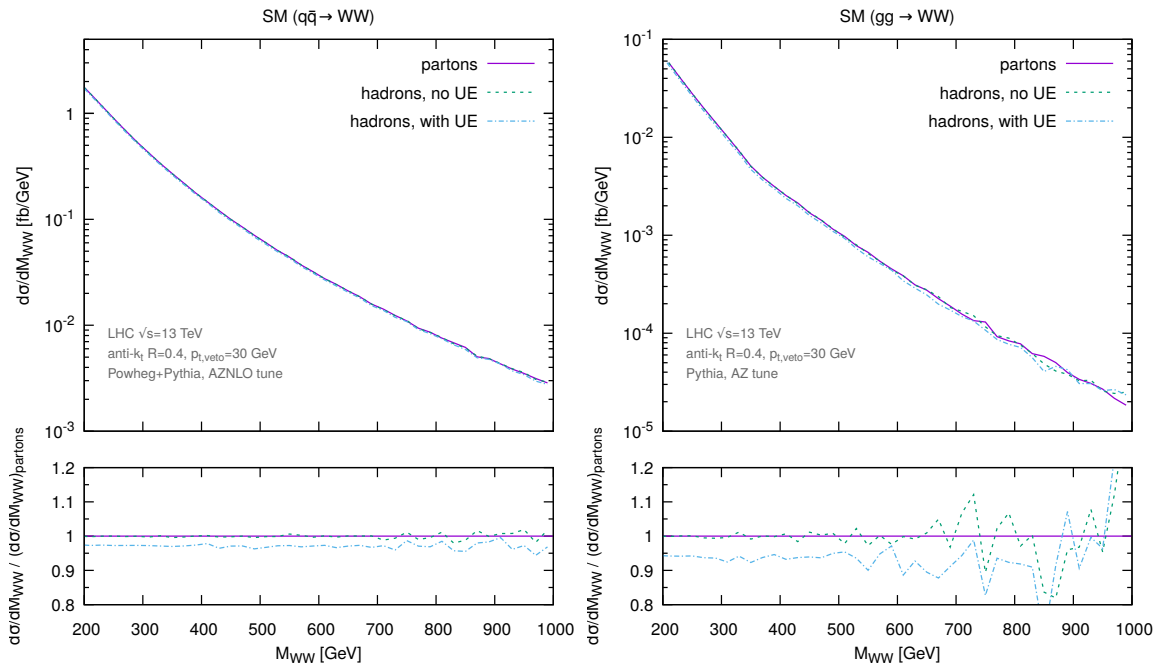


Figure 10. Impact of hadronisation and underlying event on $d\sigma/dM_{WW}$ in the SM for $q\bar{q}$ (left) modelled with POWHEG+PYTHIA and gg (right) modelled with plain PYTHIA. The fluctuations in the right plot are due to statistical uncertainties in the Monte Carlo samples.

of order $\exp[-C(\alpha_s/\pi)\Delta y \ln(30 \text{ GeV}/25 \text{ GeV})]$ ⁷, with $C = C_F$ or $C = C_A$ according to whether we have quarks or gluons in the initial state and Δy the size of rapidity region in which the jet veto cuts differ, in this case $\Delta y = 5$. This contribution is formally NNLL, because the rapidity region where ATLAS applies a more stringent jet-veto cut does not increase with increasing M_{WW} , for fixed $p_{t,\text{veto}}$. Last, the definition of $\cancel{E}_{T,\text{Rel}}$ used to define the cuts in table 1 considers only leptons, whereas ATLAS considers all reconstructed particles, including jets. This leads to small NNLL corrections that depend on the area in the y - ϕ plane occupied by the rejected jets. We study these effects using parton-shower event generators. In particular, in fig. 9 we assess the impact of different cuts on the jets on $d\sigma/dM_{WW}$, using parton shower event generators at parton level, in particular we use POWHEG+PYTHIA for $q\bar{q}$ and plain PYTHIA for gg . We observe that the rapidity cut $|y| < 4.5$ has essentially no effect. On the contrary, implementing the full ATLAS cuts gives a sizeable but constant extra suppression. This is reasonable given that the jet veto cut imposed by ATLAS in the central region $|y| < 2.5$ is tighter than the one corresponding to our simplified cuts. Although the contribution we miss is formally NNLL, for the values of M_{WW} we consider here, the rapidity region in which $p_{t,\text{veto}} = 25 \text{ GeV}$ is larger than that where $p_{t,\text{veto}} = 30 \text{ GeV}$. Therefore, using our simplified cuts to mimic the ATLAS

⁷This naive estimate neglects the so-called non-global logarithms [71].

cuts we miss a potentially large contribution. In the case of gg , the suppression is larger with respect to $q\bar{q}$ due to the larger colour factor of the initial-state gluons with respect to the quarks.

Last, in fig. 10 we investigate the impact on $d\sigma/dM_{WW}$ of non-perturbative corrections due to hadronisation and underlying event, using parton shower event generators. Again we make use of POWHEG+PYTHIA for $q\bar{q}$ and plain PYTHIA for gg . We observe that hadronisation corrections are essentially negligible, which is expected since they scale like inverse powers of the hard scale, in this case M_{WW} . Corrections arising from the underlying event are a few percent, smaller than the typical theoretical uncertainties of our predictions.

To summarise, the effect with the greatest impact is the different jet-veto procedure employed by ATLAS. This could be modelled more accurately, either by making use of an effective $p_{t,\text{veto}}$, or even better by performing a resummation of jet-veto effects with rapidity cuts, as done in [72]. Both improvements are beyond the scope of the present work.

5 Sensitivity studies

In this section, we compare the sensitivity of WW and ZZ production at HL-LHC ($\sqrt{s} = 14 \text{ TeV}$, with 3 ab^{-1} of integrated luminosity) to the BSM operator considered in eq. (1.1). Here we consider only the decay $ZZ \rightarrow e^+e^-\mu^+\mu^-$. First we present the best predictions that could be obtained with the theoretical tools considered here, for a given choice of observables for the two processes. For WW we choose M_{T1} in eq. (4.5a), and our best prediction is NNLL for $q\bar{q} \rightarrow WW$ and NLL for $gg \rightarrow WW$. For ZZ we consider M_{ZZ} , and our best prediction is NLO for $q\bar{q} \rightarrow ZZ$ and LO for $gg \rightarrow ZZ$. Note that the accuracy of the predictions for $q\bar{q}$ annihilation for both WW and ZZ production can be improved to include the most recent NNLO calculations of refs. [73, 74]. For gluon fusion, full NLO corrections have yet to be calculated, although approximate results are available [75–81]. While the inclusion of NNLO corrections to ZZ is straightforward, and can be obtained by running the code MATRIX [82–87], the use of NNLO corrections to WW requires matching of fixed-order predictions to the NNLL resummation. Although this can be achieved by interfacing the NNLL resummation to MATRIX, it is technically more involved than the simple procedure described in section 3. Therefore, we leave matching to NNLO to future work. The differential distributions in M_{T1} and M_{ZZ} are shown in figure 11. We observe that, in the $q\bar{q}$ channel, the cross section $d\sigma/dM_{T1}$ with a jet-veto is comparable to the cross section $d\sigma/dM_{ZZ}$ where no jet veto is applied. We note that, even with a jet veto, the $q\bar{q}$ background is much larger in the WW case. Therefore, we naively expect WW to perform slightly worse than ZZ for exclusion of BSM effects.

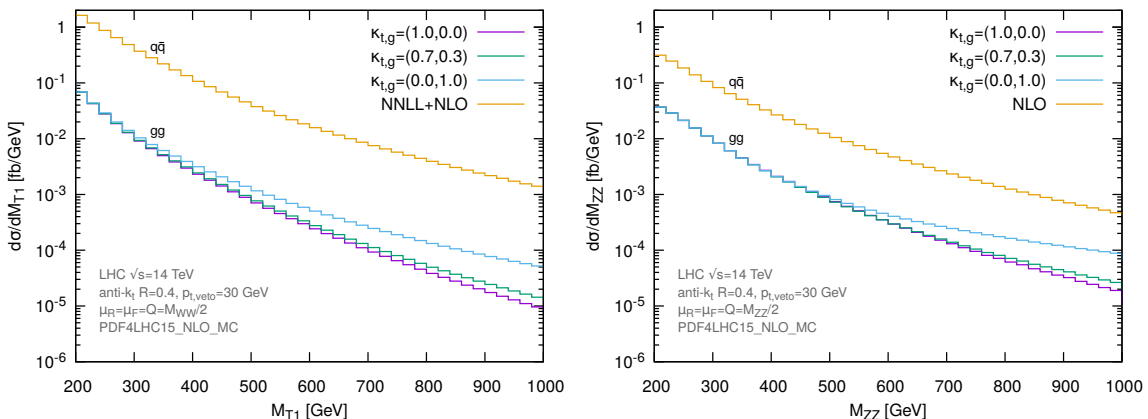


Figure 11. Our best predictions for the differential distributions $d\sigma/dM_{T1}$ for WW production with the experimental cuts in table 1 (left) and $d\sigma/dM_{ZZ}$ for ZZ production with the cuts in ref. [88] (right) for $q\bar{q}$ and gg processes.

To be more quantitative, we generate exclusion plots for a range of values of the parameters κ_t and κ_g entering the Lagrangian of eq. (4.2). To do this we ask ourselves how likely it is that predictions corresponding to different values of (κ_t, κ_g) are compatible with data that agree with the SM. Quantitatively, given a value of (κ_t, κ_g) , we compute $n_i(\kappa_t, \kappa_g)$, the expected number of events in bin i of the distribution in a suitable leptonic observable. Specifically, we choose M_{T1} for WW production and M_{ZZ} for ZZ . Given a set of data points $\{n_i\}_{i=1,\dots,N}$, and a given value of (κ_t, κ_g) , we define

$$\chi^2(\kappa_t, \kappa_g) \equiv \sum_i \frac{(n_i(\kappa_t, \kappa_g) - n_i)^2}{n_i}, \quad (5.1)$$

and from that we construct our test statistic

$$\Delta\chi^2(\kappa_t, \kappa_g) \equiv \chi^2(\kappa_t, \kappa_g) - \chi^2(\hat{\kappa}_t, \hat{\kappa}_g), \quad (5.2)$$

where $(\hat{\kappa}_t, \hat{\kappa}_g)$ are the values of (κ_t, κ_g) that minimise $\chi^2(\kappa_t, \kappa_g)$. This test statistic is a good approximation to the usual log-likelihood ratio for counting experiments [89] in the limit of a large number of events, and in the assumption that there are no correlations between bins. Assuming $n_i(\kappa_t, \kappa_g)$ is the expected number of events, in the denominator of eq. (5.1) we can approximate $n_i \simeq n_i(\kappa_t, \kappa_g)$. Therefore, $\Delta\chi^2(\kappa_t, \kappa_g)$ is asymptotically distributed according to a chi-squared distribution with two degrees of freedom (see e.g. [90]), which we denote by $f(\Delta\chi^2(\kappa_t, \kappa_g) | \kappa_t, \kappa_g)$.

We now consider data $\{n_i\}_{i=1,\dots,N}$ generated in such a way that the expected number of events in each bin is the “central” SM prediction, corresponding to $\mu_R = \mu_F = Q = M_{WW}/2$ for WW and $\mu_R = \mu_F = M_{ZZ}/2$ for ZZ , which we denote with $\bar{n}_i(1, 0)$. This constitutes our “background-only” hypothesis. We now set exclusion

limits in the (κ_t, κ_g) plane using the median significance [89, 91], assuming those data, with which one rejects the hypothesis corresponding to each value of (κ_t, κ_g) (our “signal” hypothesis). More precisely, for each value of (κ_t, κ_g) , we construct the distribution in $\Delta\chi^2(\kappa_t, \kappa_g)$ under the assumption of the background-only hypothesis, which we denote by $f(\Delta\chi^2(\kappa_t, \kappa_g) \mid 1, 0)$. We then compute the median of that distribution, which we denote with $\Delta\chi_{\text{med}}^2(\kappa_t, \kappa_g)$. The p -value for each (κ_t, κ_g) is given by

$$p(\kappa_t, \kappa_g) = \int_{\Delta\chi_{\text{med}}^2(\kappa_t, \kappa_g)}^{\infty} f(\Delta\chi^2 \mid \kappa_t, \kappa_g) d(\Delta\chi^2), \quad (5.3)$$

and we exclude at the 95% confidence level all (κ_t, κ_g) such that $p(\kappa_t, \kappa_g) < 0.05$. In practice, we have binned the variables M_{T1} and M_{ZZ} in such a way that, when computing $\Delta\chi_{\text{med}}^2(\kappa_t, \kappa_g)$, in the denominator of eq. (5.1) we can always approximate n_i with $\bar{n}_i^{q\bar{q}}$, the number of events obtained using central scales and the $q\bar{q}$ subprocess only.

We first consider the case in which the expected number of events for the signal hypothesis corresponds to $\bar{n}_i(\kappa_t, \kappa_g)$. We have examined two cases, both corresponding to di-boson invariant masses above the Higgs mass, so as to ensure to have complementary information with respect to Higgs cross sections. In one case, we have considered only two bins, a low-mass bin ($200 \text{ GeV} < M_{T1}, M_{ZZ} < 400 \text{ GeV}$) and a high-mass bin containing the rest of the distributions. The low-mass bin is more sensitive to κ_t , and the high-mass bin to κ_g . The corresponding exclusion regions in the (κ_t, κ_g) plane are bounded by the dashed contours in Fig. 12. We see that WW is complementary to ZZ for low values of κ_t , whereas the sensitivity to κ_g of ZZ is larger. This can be understood from figure 11. Note that, despite the fact that the WW cross-section is larger, the presence of the jet veto kills a good fraction of the gg signal, with the net effect that its cross-section decreases with increasing M_{T1} . In the ZZ case, where there is no suppression due to a jet veto, the contact interaction driven by κ_g is fully effective, and makes the gg signal flatter with respect to the $q\bar{q}$ background, thus giving a larger sensitivity to κ_g . We gain sensitivity by considering a greater number of bins. For instance, we have considered 60 bins equally spaced from 200 GeV to 1400 GeV, and an extra bin containing the distribution with larger values of M_{T1} or M_{ZZ} . The corresponding exclusion contours are the solid lines in Fig. 12. For reference, we also plot the line $\kappa_t + \kappa_g = 1$, and three points corresponding to the SM, and the scenarios BSM_1 and BSM_2 considered in the previous section. We also draw bands corresponding to 95% confidence-level bounds on $\kappa_t + \kappa_g$ and κ_t obtained from ref. [92]. These give more stringent constraints than our observables, which have nevertheless complementary sensitivity, since the analysis of ref. [92] probes regions of di-boson invariant masses that we do not consider here. Also, having full control of theoretical predictions for both the signal and the background, our procedure is suitable for optimisation of both the observables and the binning procedure, and is open to improvements of the theoretical predictions.

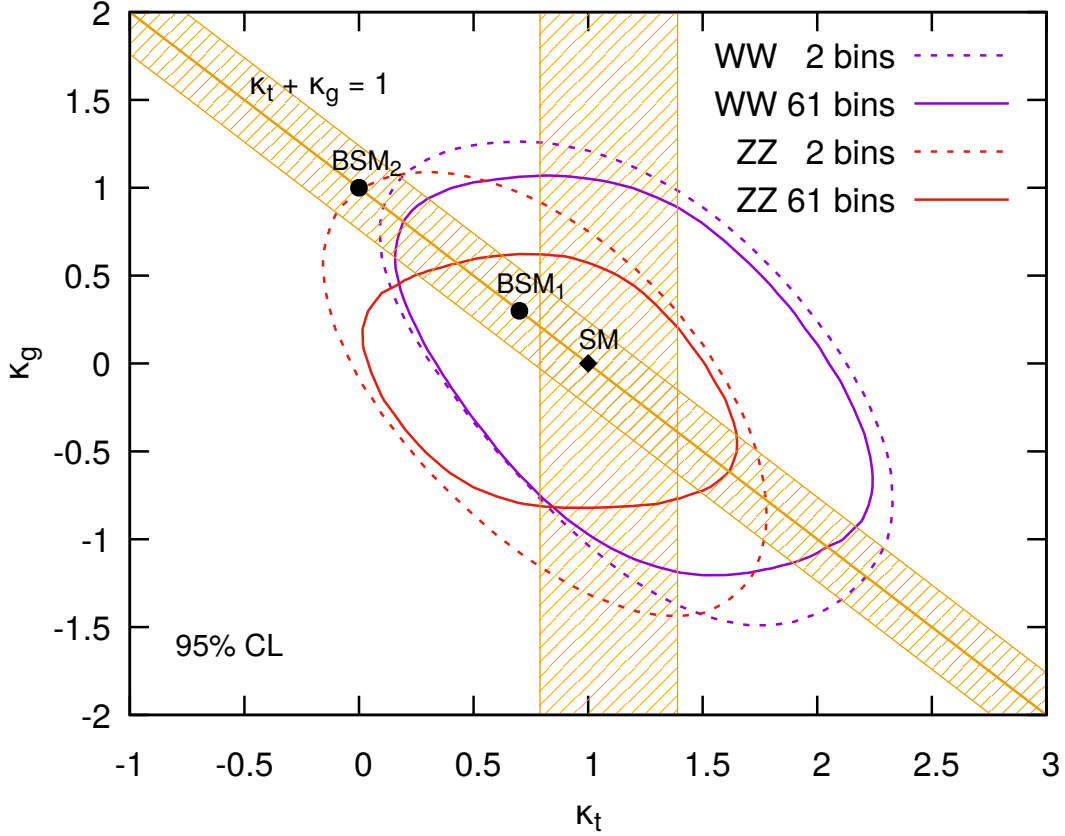


Figure 12. Exclusion contours at 95% level for WW and ZZ production. See the main text for details.

The exclusion contours we have obtained so far do not take into account theoretical uncertainties. Including theoretical uncertainties, the true theory value $n_i(\kappa_t, \kappa_g)$ will differ from its central prediction $\bar{n}_i(\kappa_t, \kappa_g)$ by some theoretical error δ_i , taken to lie in some interval Δ_i . In every bin, $n_i(\kappa_t, \kappa_g)$ will be the sum of a contribution $n_i^{(q\bar{q})}$ arising from quark-antiquark annihilation, and a contribution $n_i^{(gg)}(\kappa_t, \kappa_g)$ arising from gluon fusion. Denoting by $\Delta_i^{(gg)}(\kappa_t, \kappa_g)$ and $\Delta_i^{(q\bar{q})}$ the theoretical uncertainties on (respectively) $n_i^{(gg)}(\kappa_t, \kappa_g)$ and $n_i^{(q\bar{q})}$, and considering the fact that these predictions correspond to completely uncorrelated processes, we take the theoretical uncertainty on $n_i(\kappa_t, \kappa_g)$ to be given by

$$\Delta_i(\kappa_t, \kappa_g) = \sqrt{\left(\Delta_i^{(gg)}(\kappa_t, \kappa_g)\right)^2 + \left(\Delta_i^{(q\bar{q})}\right)^2}. \quad (5.4)$$

Therefore, the χ^2 corresponding to a given value of $(\kappa_t, \kappa_g, \vec{\delta} \equiv \{\delta_1, \delta_2, \dots\})$ is given

by

$$\chi_{\text{exp}}^2(\kappa_t, \kappa_g, \vec{\delta}) \equiv \sum_i \frac{(\bar{n}_i(\kappa_t, \kappa_g) + \delta_i - n_i)^2}{n_i}. \quad (5.5)$$

In order to estimate the impact of theoretical uncertainties on our sensitivity contours, we adopt the approach of ref. [90], and add to χ_{exp}^2 a Gaussian “theory term”, with a width $\Delta_i(\kappa_t, \kappa_g)/2$, as follows:

$$\chi_{\text{th}}^2(\kappa_t, \kappa_g, \vec{\delta}) \equiv \sum_i \frac{\delta_i^2}{(\Delta_i(\kappa_t, \kappa_g)/2)^2}. \quad (5.6)$$

The test statistic corresponding to (κ_t, κ_g) is then obtained by profiling with respect to $\vec{\delta}$, i.e. computing

$$\chi^2(\kappa_t, \kappa_g) \equiv \min_{\vec{\delta}} \left[\chi_{\text{exp}}^2(\kappa_t, \kappa_g, \vec{\delta}) + \chi_{\text{th}}^2(\kappa_t, \kappa_g, \vec{\delta}) \right]. \quad (5.7)$$

For χ_{exp}^2 and χ_{th}^2 as in (5.5) and (5.6) this gives

$$\chi^2(\kappa_t, \kappa_g) = \sum_i \frac{(\bar{n}_i(\kappa_t, \kappa_g) - n_i)^2}{n_i + (\Delta_i(\kappa_t, \kappa_g)/2)^2}. \quad (5.8)$$

In other words, for a Gaussian theory term our treatment is equivalent to the common prescription to combine theoretical and experimental errors in quadrature.⁸ With our choice of bins, we can approximate $\Delta_i(\kappa_t, \kappa_g) \simeq \Delta_i^{(q\bar{q})}$.

Before presenting sensitivity contours including theory uncertainties, it is worth comparing the impact of statistical and theoretical uncertainties. In the case of WW production, theory uncertainties differ according to whether we use the efficiency method described in appendix A.3, or we just perform 9-point scale variations in the resummed cross section. In the former case, as can be seen from Fig. 7, relative theory uncertainties are of order 40%, whereas in the latter they are of order 10%, with a mild dependence on M_{WW} . In both cases then $\Delta_i^{(q\bar{q})}$ roughly scales like n_i . Therefore, by looking at the denominator of eq. (5.8), we see that in the bins with larger n_i , theory uncertainties will dominate over statistical uncertainties ($\sim \sqrt{n_i}$), and hence these bins have very little power to constrain (κ_t, κ_g) . In the case of ZZ , theory uncertainties are smaller, around 5%, so all bins retain their constraining power. This is illustrated in Fig. 13. All contours have been obtained with 61 bins, as explained above. The outer contour (dotted) corresponds to WW production with theory uncertainties estimated with the JVE method. As explained in sec. 4, the method is

⁸In fact, (5.6) itself can similarly be obtained as follows: (i) introduce separate $\delta_i^{(gg)}$ and $\delta_i^{(q\bar{q})}$ parameters for the two components of $n_i(\kappa_t, \kappa_g)$, (ii) add separate Gaussian theory terms for the former, of respective widths $\Delta_i^{(gg)}/2$ and $\Delta_i^{(q\bar{q})}/2$, (iii) define $\delta_i = \delta_i^{(gg)} + \delta_i^{(q\bar{q})}$ and rewrite the χ^2 in terms of δ and $\delta_i^{(q\bar{q})}$, (iv) profile (minimise) the χ^2 with respect to $\delta_i^{(q\bar{q})}$. This again gives the expression (5.8).

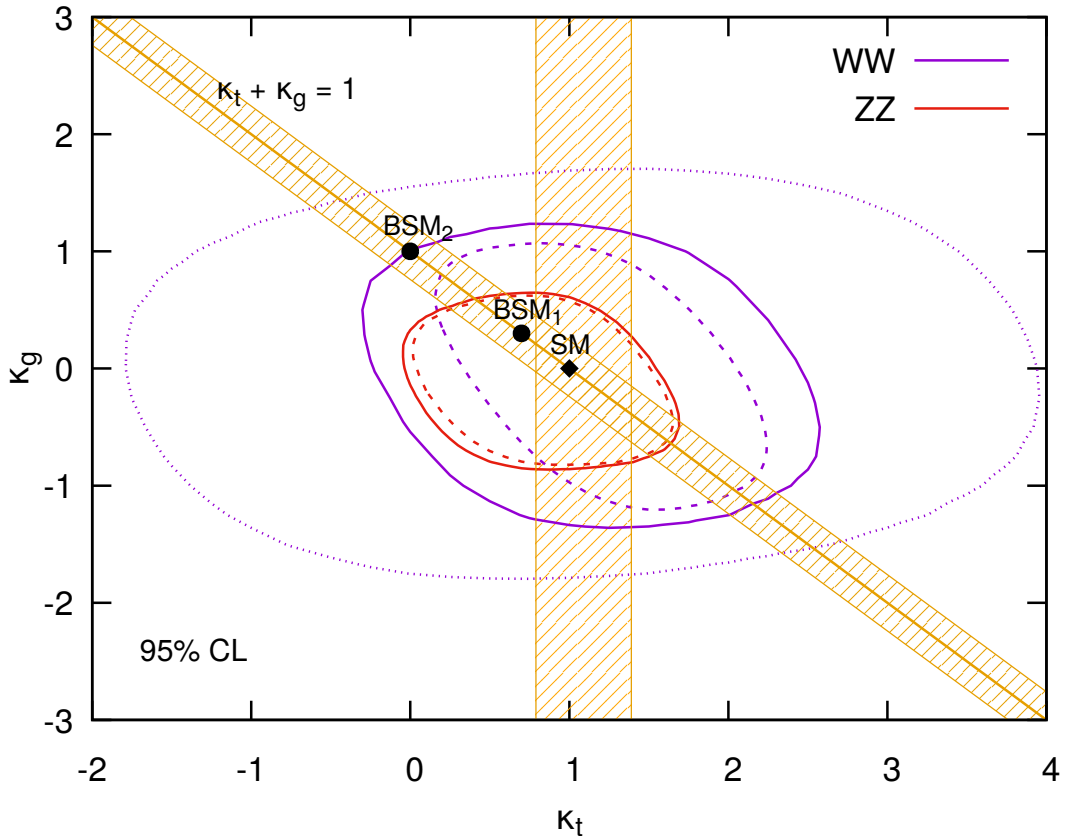


Figure 13. Exclusion contours at 95% level for WW and ZZ production, corresponding to different ways of estimating theoretical uncertainties, see the main text for details.

probably overly conservative, and the corresponding contour cannot compete with the constraints from ZZ production. Note in particular that large theoretical uncertainties affect mostly the bins with lowest values of M_{T1} , which are the most sensitive to κ_t . This explains why the JVE contour is so wide compared to the others. The solid contours correspond to uncertainties obtained with the appropriate scale variations, both for WW and for ZZ . Based on previous works on Higgs production with a jet-veto [36, 42, 50], we believe that scale variations for WW give a realistic estimate of the best theoretical uncertainties that could be obtained with a matching to NNLO with the JVE method. We see that, taking into account theory uncertainties at the currently achievable accuracy, WW does not have complementary constraining power with respect to ZZ . However, the dashed curves, corresponding to all predictions fixed at their central value without theory uncertainties, show that WW might compete with ZZ . We have therefore determined the necessary accuracy on WW production such that one obtains a comparable sensitivity with ZZ . First, we have observed that, in the case of ZZ , adding the NNLO contribution to $q\bar{q}$ does not improve the overall theory accuracy, due to missing higher orders in the gg channel.

So we assume that the uncertainties on ZZ production will remain the NLO ones, i.e. around 5%. The solid contour for WW in Fig. 14 corresponds to an estimated

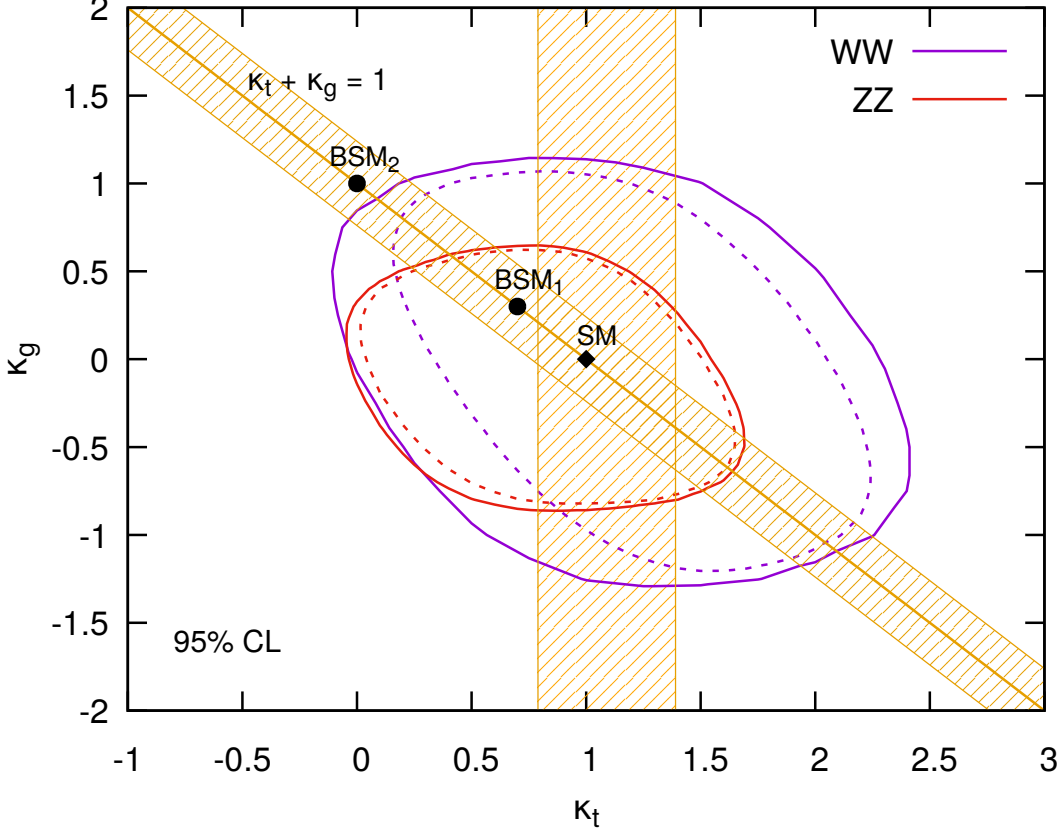


Figure 14. Exclusion contours at 95% level for WW and ZZ production, corresponding to an optimistic reduction of theoretical uncertainties, see the main text for details.

theoretical uncertainty of 3% in every bin, which is approximately the one you need for WW to be competitive with current ZZ predictions. Based again on previous work on Higgs production [50], such an uncertainty could be reached by matching NNLL resummation to a future NNLO calculation for WW plus one jet, and maybe even further decreased after an N^3LL resummation. We note that improving ZZ predictions hardly offers any stronger constraint. However, improved predictions for the gg channel, both for WW and ZZ , might move the central prediction, and may open up further space for constraints.

We conclude this section with a comment on the actual implementation of the calculation of $\chi^2(\kappa_t, \kappa_g)$. If we consider the numerator of $\chi^2(\kappa_t, \kappa_g)$ in eqs. (5.1) and (5.8), we see that it involves $n_i^{(gg)}(\kappa_t, \kappa_g)$. This quantity is a second-order polynomial in κ_t and κ_g , arising from the square of the matrix element

$$M_{SM}^{(gg)} + M_{BSM}^{(gg)} = \kappa_t M_t^{(gg)} + \kappa_g M_g^{(gg)} + M_c^{(gg)}, \quad (5.9)$$

where $M_t^{(gg)}$ and $M_g^{(gg)}$ are the contributions of the Higgs produced via a top loop and a contact interaction respectively, and $M_c^{(gg)}$ the remaining contributions, giving rise to the so-called “continuum” background. The fact that we have full control over $M^{(gg)}$ allows us to compute the coefficient of each power of κ_t and κ_g separately, and once and for all. This is crucial for an accurate calculation of $\chi^2(\kappa_t, \kappa_g)$, because a naive implementation of this quantity might involve cancellations between large numbers, whose control requires Monte Carlo samples with large statistics.

6 Conclusions

We have studied the impact of a veto on additional jets on setting limits on the coupling of a dimension-6 operator affecting WW production. In the presence of such a veto, large logarithms of the ratio of the maximum allowed jet transverse momentum $p_{t,\text{veto}}$ and the invariant mass of the WW pair M_{WW} have to be resummed at all orders in QCD. These logarithmically enhanced contributions give rise to the so-called Sudakov suppression of cross sections with respect to naive Born-level predictions. The dimension-6 operator we considered affects WW production via gluon fusion, but does not affect WW production via quark-antiquark annihilation, which stays unchanged with respect to the SM. At Born level, the effect of this operator amounts to a growth of the cross section at large values of M_{WW} . Unfortunately, the suppression due to the jet-veto gets larger with increasing M_{WW} . Also, such suppression affects gluon fusion more than quark-antiquark annihilation due to the fact that gluons radiate roughly twice as much as quarks, so vetoing radiation off gluons cuts a larger portion of cross sections. Therefore, enhancement due to a contact interaction and Sudakov suppression are in competition.

To investigate quantitatively the impact of a jet veto on WW production, we have devised a new method to interface resummed predictions for the gg and $q\bar{q}$ channels to fixed-order QCD event generators. This procedure provides events that are fully differential in the decay products of the WW pair, so that suitable acceptance cuts can be applied. The method involves minimal modifications of the ingredients already present in fixed-order event generators, and can be applied to the production of any colour singlet. In particular, we have implemented the procedure in the fixed-order program MCFM, which resulted in the code we called MCFM-RE, a Resummation Edition of MCFM.

Our program MCFM-RE has been used to produce differential cross sections for WW production with a simplified version of the ATLAS acceptance cuts, both in the SM, and including BSM effects induced by the aforementioned dimension-6 contact interaction. The main message is that, with the value of $p_{t,\text{veto}}$ used in current analyses, Sudakov suppression effects dominate over the enhancement produced by a contact interaction, so that deviations from the Standard Model are in general quite small for reasonable values of the strength of the contact interaction.

We have compared our results with those obtained from a number of parton-shower event generators, and we have found very good agreement. We have used parton-shower event generators to estimate effects that cannot be taken into account by our analytical calculation, and found that they have a small impact, well within our theory uncertainties. We emphasise that our predictions have the computational cost of a Born-level event generator, and provide full analytical control of theoretical uncertainties. Our predictions are also in agreement, within uncertainties, with those obtained by interfacing a SCET calculation with the same formal accuracy with `aMC@NLO`.

We produced projections for the sensitivity to the considered BSM effects for HL-LHC, and compared with what could be obtained using ZZ production, which is not affected by the presence of a jet veto. We have found that WW has complementary sensitivity, provided it is possible to reduce theory uncertainties below 3%. This could be achieved by both matching current resummed predictions with a future calculation of WW plus one jet at NNLO, and improving the resummation to achieve N³LL accuracy. We hope this work encourages further theoretical work in both directions. We remark that the main advantage of using `MCFM-RE` for such studies compared to parton-shower event generators is that we have access to amplitudes, so we can compute separately all terms contributing to square matrix elements, in particular interference terms which can be computed separately with an arbitrary numerical accuracy.

We have found that, with the current acceptance cuts, the observables we have considered are not yet competitive with Higgs total cross sections, although they do provide additional information. However, our code does provide an accurate and fast tool to explore different choices of cuts and observables, so could be used for further studies in this direction. In fact, with minimal modifications, it can also produce predictions with event-by-event jet vetoes, as proposed in [93, 94]. Furthermore, our code is open to the implementation of other models of new physics affecting the production of a colour singlet.

Last, our code is the only implementation of the jet-veto resummation of ref. [50] that is fully exclusive in the decay products of a colour singlet, so it can be used for precision determinations of Standard Model parameters, notably those characterising the Higgs boson.

Acknowledgments

We are grateful to Tilman Plehn for suggesting a reference and to Christian Reuschle for extensive advice on configuring `HERWIG` as well as Keith Hamilton, Simon Plätzer and Peter Richardson for useful comments on `HERWIG`-related issues. We also acknowledge useful discussions on statistics with Luiz Vale Silva, and on the effect of rapidity cuts on jet-veto resummations with Johannes Michel and Frank Tackmann.

N.K. would like to thank CERN for hospitality and partial financial support through the CERN Theory Institute on *LHC and the Standard Model: Physics and Tools*. This work was supported in part by STFC grant ST/P000738/1.

A Collection of relevant formulae

In this appendix we report the explicit expressions that we have implemented in MCFM to achieve NLL and NNLL resummation of the cross section for the production of a colour singlet with a jet-veto. This discussion is of a technical nature, and we assume that the reader is familiar with the details of the jet-veto resummations performed in refs. [36, 42, 50].

In general, we consider the production of a colour singlet of invariant mass M , for instance a Higgs, a Z boson, or a pair of W bosons. At Born-level, this proceeds via either $q\bar{q}$ annihilation or gluon fusion. We then compute the cross section $d\sigma_{\text{i.s.}}/(dM^2 d\Phi_n)$, with i.s. = $q\bar{q}, gg$, fully differential in the phase space of the decay products of the colour singlet. Given their momenta q_1, q_2, \dots, q_n , and incoming momenta p_1 and p_2 , the phase space $d\Phi_n$ is defined as

$$d\Phi_n = \prod_{i=1}^n \frac{d^3\vec{q}_i}{(2\pi)^3 2E_i} (2\pi)^4 \delta\left(p_1 + p_2 - \sum_{i=1}^n q_i\right), \quad (\text{A.1})$$

with E_i and \vec{q}_i the energy and three-momentum of particle q_i .

Any prediction for $d\sigma_{\text{i.s.}}/(dM^2 d\Phi_n)$ depends on the renormalisation scale μ_R at which we evaluate the strong coupling α_s , as well as the factorisation scale μ_F at which we evaluate the PDFs. Both scales are typically set at values of order M . Furthermore, in the presence of a jet-veto, $d\sigma_{\text{(i.s.)}}/(dM^2 d\Phi_n)$ is affected by large logarithms $L \equiv \ln(M/p_{\text{t,veto}})$, with $p_{\text{t,veto}}$ the maximum allowed transverse momentum of the observed jets. When resumming such logarithms at all orders, our predictions become functions of \tilde{L} , defined as

$$\tilde{L} = \frac{1}{p} \ln\left(\left(\frac{Q}{p_{\text{t,veto}}}\right)^p + 1\right). \quad (\text{A.2})$$

The quantity \tilde{L} is such that for large $p_{\text{t,veto}}$, $\tilde{L} \rightarrow 0$, which implements the fact that, in this regime, there are no large logarithms to be resummed. Also, at small $p_{\text{t,veto}}$, $\tilde{L} \simeq \ln(Q/p_{\text{t,veto}})$, so in fact we resum logarithms of the ratio of $p_{\text{t,veto}}$ and the so-called resummation scale Q . The three scales μ_R, μ_F, Q are handles that we will use to estimate theoretical uncertainties, as explained in app. A.3. The power p determines how fast the resummation switches off at large $p_{\text{t,veto}}$. We choose $p = 5$, as in refs. [36, 42, 50].

A.1 NLL resummation

At NLL accuracy, the distribution $d\sigma_{\text{i.s.}}/(dM^2 d\Phi_n)$ is given by

$$\frac{d\sigma_{\text{i.s.}}^{\text{NLL}}}{dM^2 d\Phi_n} = \mathcal{L}_{\text{i.s.}}^{(0)}(\tilde{L}, M) e^{\tilde{L}g_1(\alpha_s \tilde{L}) + g_2(\alpha_s \tilde{L})}, \quad \alpha_s = \alpha_s(\mu_R). \quad (\text{A.3})$$

Explicit expressions for the functions g_1, g_2 can be found in the supplemental material of ref. [36]. The NLL ‘‘luminosity’’ $\mathcal{L}_{\text{i.s.}}^{(0)}(L, M)$ is given by

$$\mathcal{L}_{\text{i.s.}}^{(0)}(L, M) \equiv \sum_{i,j} \int dx_1 dx_2 \left| M_{ij}^{(\text{i.s.})} \right|^2 \delta(x_1 x_2 s - M^2) f_i(x_1, \mu_F e^{-L}) f_j(x_2, \mu_F e^{-L}). \quad (\text{A.4})$$

In the above expression, $M_{ij}^{(\text{i.s.})}$ is the Born-level amplitude for the production of the colour singlet via annihilation of the two partons i and j , and $f_{i,j}$ is the density of parton i, j in the proton.

Given any Born-level event generator, the recipe to implement the NLL resummation of eq. (A.3) is straightforward:

1. change the factorisation scale μ_F provided by the generator to $\mu_F e^{-\tilde{L}}$;
2. multiply the weight of every event by a factor $\exp \left[\tilde{L}g_1(\alpha_s \tilde{L}) + g_2(\alpha_s \tilde{L}) \right]$.

Note that, if $p_{\text{t,veto}}$ is fixed, and we do not integrate over different values of M^2 , both operations can be performed without touching the Born-level generator code. In fact, many programs allow a change in the factorisation scale by a constant factor. Also, the rescaling of the weight can be performed by the analysis routines that produce histograms for physical distributions. In our implementation, since we do want to integrate over M^2 , we have implemented the change in factorisation scale inside the MCFM code.

Another advantage we have in using MCFM is that it gives us access to the matrix elements in a form that is human readable. This is particularly useful in case one wishes to separate contributions from different parts of the matrix element, for instance a possible BSM contribution from that of the SM background. We consider here the case of WW production via gluon fusion, but the argument applies to other processes as well. There, the Born-level matrix element has the form $M^{(gg)} = M_{\text{SM}}^{(gg)} + M_{\text{BSM}}^{(gg)}$, where $M_{\text{SM}}^{(gg)}$ is the SM amplitude, and $M_{\text{BSM}}^{(gg)}$ a BSM contribution. For each phase space point, we can then isolate individual contributions to the luminosity by computing separately each term in the square

$$|M^{(gg)}|^2 = |M_{\text{SM}}^{(gg)}|^2 + |M_{\text{BSM}}^{(gg)}|^2 + 2\text{Re} \left[M_{\text{SM}}^{(gg)} \left(M_{\text{BSM}}^{(gg)} \right)^* \right]. \quad (\text{A.5})$$

In the specific case, given the expression of $M^{(gg)}$ in eq. (5.9), we compute the luminosity $\mathcal{L}_{gg}^{(0)}(L, M)$ as follows

$$\begin{aligned} \mathcal{L}_{gg}^{(0)}(L, M) = & \kappa_t^2 \mathcal{L}_{gg}^{(t^2)}(L, M) + \kappa_g^2 \mathcal{L}_{gg}^{(g^2)}(L, M) + \kappa_t \kappa_g \mathcal{L}_{gg}^{(tg)}(L, M) + \\ & + \kappa_t \mathcal{L}_{gg}^{(tc)}(L, M) + \kappa_g \mathcal{L}_{gg}^{(gc)}(L, M) + \mathcal{L}_{gg}^{(c^2)}(L, M), \end{aligned} \quad (\text{A.6})$$

where we have used the notation

$$\mathcal{L}_{gg}^{(i^2)}(L, M) = \int dx_1 dx_2 \left| M_i^{(gg)} \right|^2 \delta(x_1 x_2 s - M^2) f_g(x_1, \mu_F e^{-L}) f_g(x_2, \mu_F e^{-L}), \quad (\text{A.7})$$

with $i = t, g, c$, and

$$\begin{aligned} \mathcal{L}_{gg}^{(ij)}(L, M) = & \int dx_1 dx_2 2\text{Re} \left[M_i^{(gg)} \left(M_j^{(gg)} \right)^* \right] \delta(x_1 x_2 s - M^2) \times \\ & \times f_g(x_1, \mu_F e^{-L}) f_g(x_2, \mu_F e^{-L}), \end{aligned} \quad (\text{A.8})$$

with $ij = tg, tc, gc$. Using these luminosities we can interpret $\mathcal{L}_{gg}^{(0)}$ as a polynomial in the various κ_i , and compute each coefficient separately. All one has to do then is to reweight each phase-space point using the Sudakov exponent $\exp \left[\tilde{L} g_1(\alpha_s \tilde{L}) + g_2(\alpha_s \tilde{L}) \right]$. In doing so, we have used the fact that the Sudakov exponent depends only on the colour and kinematics of the incoming partons, and therefore is the same for every single contribution to the luminosity.

A.2 NNLL resummation

At NNLL accuracy, the cross section $d\sigma_{\text{i.s.}}/(dM^2 d\Phi_n)$ with a jet veto is given by

$$\begin{aligned} \frac{d\sigma_{\text{i.s.}}^{\text{NNLL}}(p_{t,\text{veto}})}{dM^2 d\Phi_n} = & \left(\mathcal{L}_{\text{i.s.}}^{(0)}(\tilde{L}, M) + \mathcal{L}_{\text{i.s.}}^{(1)}(\tilde{L}, M) \right) \times \\ & \times \left(1 + \mathcal{F}_{\text{clust}}(R) + \mathcal{F}_{\text{correl}}(R) \right) \times e^{\tilde{L} g_1(\alpha_s \tilde{L}) + g_2(\alpha_s \tilde{L}) + \frac{\alpha_s}{\pi} g_3(\alpha_s \tilde{L})}, \end{aligned} \quad (\text{A.9})$$

where the function g_3 can be found in ref. [36]. The functions $\mathcal{F}_{\text{clust}}(R), \mathcal{F}_{\text{correl}}(R)$ depend on the jet radius R . Their expressions can be found in ref. [42]. As for the NLL resummation, $\alpha_s = \alpha_s(\mu_R)$. The remaining new ingredient for NNLL resummation is the luminosity $\mathcal{L}_{\text{i.s.}}^{(1)}(L, M)$, defined as

$$\begin{aligned} \mathcal{L}_{\text{i.s.}}^{(1)}(L, M) = & \sum_{i,j} \int dx_1 dx_2 |M_{ij}^{(\text{i.s.})}|^2 \delta(x_1 x_2 s - M^2) \frac{\alpha_s}{2\pi} \left[\mathcal{H}_{\text{i.s.}}^{(1)} f_i(x_1, \mu_F e^{-L}) f_j(x_2, \mu_F e^{-L}) \right. \\ & \left. + \frac{1}{1 - 2\alpha_s \beta_0 L} \sum_k \left(\int_{x_1}^1 \frac{dz}{z} C_{ik}^{(1)}(z) f_k\left(\frac{x_1}{z}, \mu_F e^{-L}\right) f_j(x_2, \mu_F e^{-L}) + \{(x_1, i) \leftrightarrow (x_2, j)\} \right) \right], \end{aligned} \quad (\text{A.10})$$

with $\beta_0 = (11C_A - 2n_f)/(12\pi)$. Using the conventions of ref. [36], we have

$$\begin{aligned}\mathcal{H}_{q\bar{q}}^{(1)} &= H^{(1)} - 2C_F \left(\frac{3}{2} + \ln \frac{M^2}{Q^2} \right) \ln \frac{M^2}{Q^2}, \\ \mathcal{H}_{gg}^{(1)} &= H^{(1)} - 2C_A \left(2\pi\beta_0 + \ln \frac{M^2}{Q^2} \right) \ln \frac{M^2}{Q^2}.\end{aligned}\tag{A.11}$$

with $H^{(1)}$ the finite part of one-loop virtual corrections to the process in question, e.g. WW production through $q\bar{q}$ annihilation. The coefficients $C_{ij}^{(1)}$ depend on whether incoming partons i and j are quarks/antiquarks (q) or gluons (g), and are given by:

$$\begin{aligned}C_{q\bar{q}}^{(1)}(z) &= C_F \left[(1-z) - \frac{\pi^2}{12}\delta(1-z) + \left(\frac{1+z^2}{1-z} \right)_+ \ln \frac{Q^2}{\mu_F^2} \right], \\ C_{qg}^{(1)}(z) &= \frac{1}{2} \left[2z(1-z) + (1-2z(1-z)) \ln \frac{Q^2}{\mu_F^2} \right], \\ C_{gq}^{(1)}(z) &= C_F \left[z + \left(\frac{1+(1-z)^2}{z} \right) \ln \frac{Q^2}{\mu_F^2} \right], \\ C_{gg}^{(1)}(z) &= C_A \left[\left(2\pi\beta_0 - \frac{\pi^2}{12} \right) \delta(1-z) + 2 \left(\frac{z}{(1-z)_+} + \frac{1-z}{z} + z(1-z) \right) \ln \frac{Q^2}{\mu_F^2} \right].\end{aligned}\tag{A.12}$$

As explained in the previous section, the NLL luminosity $\mathcal{L}_{i.s.}^{(0)}$ can be obtained from a Born-level event generator. The function $\mathcal{L}_{i.s.}^{(1)}$ represents a correction to $\mathcal{L}_{i.s.}^{(0)}$ of relative order α_s . Therefore, its implementation requires at least a NLO generator. Any NLO event generator includes the calculation of virtual corrections, as well as integrated counterterms. This contribution, which we denote by $d\sigma_{i.s.,v+ct}^{(1)}/(d\Phi_n dM^2)$, has the same form as the luminosity $\mathcal{L}_{i.s.}^{(1)}$, but with PDFs evaluated at a different factorisation scale, and different functions replacing $\mathcal{H}_{i.s.}^{(1)}$ and $C_{ij}^{(1)}(z)$. Its expression in general depends on the way each process is implemented in the NLO event generator. For instance, the implementation of WW production in the NLO program MCFM follows from the general coding of the production of a colour singlet, whose details can be found in ref. [95]. Schematically,

$$\begin{aligned}\left(\frac{d\sigma_{i.s.,v+ct}^{(1)}}{d\Phi_n dM^2} \right)_{\text{MCFM}} &= \sum_{i,j} \int dx_1 dx_2 |M_{ij}^{(i.s.)}|^2 \delta(x_1 x_2 s - M^2) \frac{\alpha_s}{2\pi} \left[\mathcal{H}_{\text{MCFM},i.s.}^{(1)} f_i(x_1, \mu_F) f_j(x_2, \mu_F) \right. \\ &\left. + \sum_k \left(\int_{x_1}^1 \frac{dz}{z} C_{\text{MCFM},ik}^{(1)}(z) f_k\left(\frac{x_1}{z}, \mu_F\right) f_j(x_2, \mu_F) + \{(x_1, i) \leftrightarrow (x_2, j)\} \right) \right].\end{aligned}\tag{A.13}$$

After direct inspection of the MCFM code, we realised that the term $\mathcal{H}_{\text{MCFM},i.s.}^{(1)}$ does not contain just the finite part of the virtual corrections $H^{(1)}$, but also the terms $-(\pi^2/12)\delta(1-z)$ in the coefficients $C_{q\bar{q}}^{(1)}(z)$ and $C_{gg}^{(1)}(z)$, as well as terms containing $\ln(M^2/\mu_R^2)$. Keeping this in mind, to compute the luminosity $\mathcal{L}_{i.s.}^{(1)}$ through MCFM, we had to perform the following changes to the MCFM code:

1. replace $\mathcal{H}_{\text{MCFM},i.s.}^{(1)}$ as follows

$$\begin{aligned}\mathcal{H}_{\text{MCFM},q\bar{q}}^{(1)} &\rightarrow \mathcal{H}_{\text{MCFM},q\bar{q}}^{(1)} + 2C_F \left(\frac{\pi^2}{12} + \frac{3}{2} \ln \frac{Q^2}{\mu_R^2} + \frac{1}{2} \ln \frac{M^2}{\mu_R^2} - \ln^2 \frac{M^2}{Q^2} \right), \\ \mathcal{H}_{\text{MCFM},gg}^{(1)} &\rightarrow \mathcal{H}_{\text{MCFM},gg}^{(1)} + 2C_A \left(\frac{\pi^2}{12} + 2\pi\beta_0 \ln \frac{Q^2}{\mu_R^2} + \frac{1}{2} \ln \frac{M^2}{\mu_R^2} - \ln^2 \frac{M^2}{Q^2} \right); \end{aligned} \quad (\text{A.14})$$

2. modify the integrated counterterms as follows

$$C_{\text{MCFM},ij}^{(1)}(z) \rightarrow \frac{1}{1 - 2\alpha_s\beta_0\tilde{L}} C_{ij}^{(1)}(z); \quad (\text{A.15})$$

3. change the factorisation scale in all PDFs from μ_F to $\mu_F e^{-\tilde{L}}$.

Last, to implement the full NNLL resummation, we just rescale the weight of each event by the factor

$$(1 + \mathcal{F}_{\text{clust}}(R) + \mathcal{F}_{\text{correl}}(R)) e^{\tilde{L}g_1(\alpha_s\tilde{L}) + g_2(\alpha_s\tilde{L}) + \frac{\alpha_s}{\pi} g_3(\alpha_s\tilde{L})}. \quad (\text{A.16})$$

A.3 Matching to fixed order and theoretical uncertainties

Our MCFM implementation includes the matching of resummed predictions with NLO calculations. In particular, we have implemented the relevant contributions to the two multiplicative matching schemes introduced in refs. [36, 50]. At NLO, the total cross section σ_{NLO} for the production of a colour singlet, satisfying a set of kinematical cuts for its decay products, is given by

$$\sigma_{\text{NLO}} = \sigma^{(0)} + \sigma^{(1)}, \quad (\text{A.17})$$

with $\sigma^{(0)}$ its Born-level contribution, and $\sigma^{(1)}$ a correction of relative order α_s . Similarly, at NLO, the corresponding cross section with a jet-veto $\Sigma_{\text{NLO}}(p_{t,\text{veto}})$ is given by

$$\Sigma_{\text{NLO}}(p_{t,\text{veto}}) = \sigma^{(0)} + \Sigma^{(1)}(p_{t,\text{veto}}). \quad (\text{A.18})$$

For computational convenience, it is customary to introduce

$$\bar{\Sigma}^{(1)}(p_{t,\text{veto}}) = \Sigma^{(1)}(p_{t,\text{veto}}) - \sigma^{(1)}, \quad (\text{A.19})$$

which implies $\Sigma_{\text{NLO}}(p_{t,\text{veto}}) = \sigma_{\text{NLO}} + \bar{\Sigma}^{(1)}(p_{t,\text{veto}})$. We also denote by $\Sigma_{\text{N}^k\text{LL}}(p_{t,\text{veto}})$ the resummed jet-veto cross section at N^kLL accuracy, again satisfying the chosen set of kinematical cuts for the decay products of the considered colour singlet. At this order, it has the following expansion in powers of α_s :

$$\Sigma_{\text{N}^k\text{LL}}(p_{t,\text{veto}}) = \sigma_0 + \Sigma_{\text{N}^k\text{LL}}^{(1)}(p_{t,\text{veto}}). \quad (\text{A.20})$$

As in refs. [36, 50], the matching is performed at the level of the jet-veto efficiency $\epsilon(p_{t,\text{veto}})$, the fraction of events that survives the jet veto. This quantity is matched to exact NLO, as follows:

$$\epsilon^{(a)}(p_{t,\text{veto}}) = \frac{\Sigma_{\text{N}^k\text{LL}}(p_{t,\text{veto}})}{\sigma_{\text{NLO}}} \left[1 + \frac{\Sigma^{(1)}(p_{t,\text{veto}}) - \Sigma_{\text{N}^k\text{LL}}^{(1)}(p_{t,\text{veto}})}{\sigma_0 (1 + \delta\mathcal{L}_{\text{N}^k\text{LL}}(p_{t,\text{veto}}))} \right], \quad (\text{A.21a})$$

$$\epsilon^{(b)}(p_{t,\text{veto}}) = \frac{\Sigma_{\text{N}^k\text{LL}}(p_{t,\text{veto}})}{\sigma_0} \left[1 + \frac{\bar{\Sigma}^{(1)}(p_{t,\text{veto}}) - \Sigma_{\text{N}^k\text{LL}}^{(1)}(p_{t,\text{veto}})}{\sigma_0 (1 + \delta\mathcal{L}_{\text{N}^k\text{LL}}(p_{t,\text{veto}}))} \right]. \quad (\text{A.21b})$$

At NLL accuracy, $\delta\mathcal{L}_{\text{NLL}} = 0$. At NNLL accuracy, if we define $\langle\mathcal{L}^{(0)}\rangle$ and $\langle\mathcal{L}^{(1)}\rangle$ as the integral of the luminosities $\mathcal{L}^{(0)}$ and $\mathcal{L}^{(1)}$ in eqs. (A.4) and (A.10) respectively over the appropriate configurations of the decay products of the colour singlet, we have $\delta\mathcal{L}_{\text{N}^k\text{LL}}(p_{t,\text{veto}}) \equiv \langle\mathcal{L}^{(1)}\rangle / \langle\mathcal{L}^{(0)}\rangle$. Both matched efficiencies reduce to $\Sigma_{\text{N}^k\text{LL}}(p_{t,\text{veto}})/\sigma_{\text{NLO}}$ for $p_{t,\text{veto}} \ll M$, up to N³LL corrections. On the other hand, for $p_{t,\text{veto}} \sim M$, we have

$$\epsilon^{(a)}(p_{t,\text{veto}}) \simeq \frac{\Sigma_{\text{NLO}}(p_{t,\text{veto}})}{\sigma_{\text{NLO}}}, \quad \epsilon^{(b)}(p_{t,\text{veto}}) \simeq 1 - \frac{\bar{\Sigma}^{(1)}(p_{t,\text{veto}})}{\sigma_0}. \quad (\text{A.22})$$

Note also that, for $p_{t,\text{veto}} \rightarrow \infty$, both efficiencies tend to one, as is physically sensible.

In order to estimate the theoretical uncertainties on jet-veto cross sections, we adapt the jet-veto efficiency method of ref. [50] to the present situation. First, our “central” prediction is $\epsilon^{(a)}(p_{t,\text{veto}})$ with $\mu_R = \mu_F = Q = Q_0$, with $Q_0 = M/2$. Then, we vary renormalisation and factorisation scale for $\epsilon^{(a)}(p_{t,\text{veto}})$ in the range

$$\frac{1}{2} \leq \frac{\mu_{R,F}}{Q_0} \leq 2, \quad \frac{1}{2} \leq \frac{\mu_R}{\mu_F} \leq 2. \quad (\text{A.23})$$

Then, we vary the resummation scale Q for $\epsilon^{(a)}(p_{t,\text{veto}})$ in the range $2/3 \leq Q/Q_0 \leq 3/2$, with $\mu_R = \mu_F = Q_0$. In practice, we do not vary the scales continuously, but we consider only $\mu_{R,F} = \{1/2, 1, 2\}Q_0$ and $Q = \{2/3, 1, 3/2\}Q_0$. Our uncertainty band is the envelope of the curves obtained by fixing the considered scales at the boundaries of the allowed range (i.e. 9-point scale variation), plus $\epsilon^{(b)}(p_{t,\text{veto}})$ with all scales set to Q_0 .

We then compute the total cross section σ_{NLO} by choosing as our central prediction the one with both renormalisation and factorisation scales set at Q_0 . We then perform renormalisation and factorisation scale variations in the range (A.23), and constructing an uncertainty band as for the efficiency, i.e. using the values of the scales at the boundaries of the allowed region (7-point scale variation).

Last, the central value for the jet-veto cross section is defined as the product of the central prediction for σ_{NLO} and $\epsilon^{(a)}(p_{t,\text{veto}})$, and the corresponding uncertainty band is obtained by adding the uncertainties of the total cross section and the efficiency in quadrature.

If the total cross section is only available at leading-order, we perform the resummation at NLL accuracy. Since we cannot normalise resummed cross sections using σ_{NLO} , $\epsilon^{(a)}(p_{t,\text{veto}}) = \epsilon^{(b)}(p_{t,\text{veto}})$. Once we have the efficiency, we evaluate theoretical uncertainties by adding in quadrature the uncertainties on σ_{LO} and the jet-veto efficiency.

B Numerical implementation in MCFM

In this section we give the details of the implementation of the resummation of jet-veto effects for colour singlets in MCFM. We assume that the reader can successfully compile and run the MCFM code, in all its operation modes. If not, the interested reader should consult the MCFM manual [44].

B.1 Overview

MCFM-RE (an acronym for Resummation Edition) is a modification of MCFM-8.0 to include the resummation of jet-veto effects in colour-singlet processes up to NNLL+LL_R accuracy. The modifications are modular, as most of the resummation effects are included through an interface to the code JetVHeto [39], suitably modified to become a library linkable to MCFM. Although a small number of modifications require us to directly change the MCFM code, these do not interfere with its usual modes of operation. The program is available on request. Included in the package are a README file and an example input card.

To run MCFM-RE, one must simply provide a suitably modified MCFM input card. We list here the new parameters we have added or changes made to existing parameters, described with the same conventions and terminology as the MCFM manual.

- **file version number.** This should match the version number that is printed when `mcfm` is executed.

{blank line}

[Flags to specify the mode in which MCFM is run]

- **part**
 - **ll.** Jet-veto resummation at LL accuracy, i.e. each event produced by MCFM is reweighted with $\exp[\tilde{L}g_1(\alpha_s\tilde{L})]$.
 - **nll.** Jet-veto resummation at NLL accuracy, see eq. (A.3).
 - **nnll.** Jet-veto resummation at NNLL accuracy, with or without the inclusion of small jet radius resummation (LL_R), see eq. (A.9).
 - **lumi0.** Calculation of the luminosity $\mathcal{L}^{(0)}$ in eq. (A.4)

- `lumi1`. Calculation of the luminosity $\mathcal{L}^{(1)}$ in eq. (A.10)
- `nllexp1`. Expansion of the NLL resummation at order α_s (for matching).
- `nnllexp1`. Expansion of the NNLL resummation at order α_s (for matching).

{blank line}

[JetVHeto resummation options]

- `observable`.
 - `ptj`. The default mode of the resummation, resum logarithms of the jet-veto.
 - `ptj+small-r`. Available for NNLL resummations only. Include the effect of resumming the jet radius at leading logarithmic accuracy.
- `Qscale`. This parameter may be used to adjust the value of the *resummation scale* Q introduced in eq. (A.2). It behaves in the same way as the MCFM parameters `scale` and `facscale` do, i.e. if `dynamicsscale` is `.false.`, Q is set to `Qscale`, otherwise $Q = \text{Qscale} \times \mu_0$, with μ_0 the dynamic scale specified by the parameter `dynamicsscale`.
- `Rscale`. This parameter may be used to adjust the value of the jet-radius resummation scale.
- `ptjveto`. The value of the jet-veto cut $p_{t,\text{veto}}$ in units of GeV.

{blank line}

[Coupling rescaling in the kappa formalism]

- `kappa_t`. The parameter κ_t of the Lagrangian in eq. (4.2), a.k.a the anomalous top Yukawa coupling.
- `kappa_b`. Anomalous bottom Yukawa coupling.
- `kappa_g`. The parameter κ_g of the Lagrangian in eq. (4.2).
- `interference only`. Flag to control whether to compute just the interference terms, e.g. the coefficient of $\kappa_t \kappa_g$ arising from squaring the amplitude in eq. (5.9). All other coefficients can be determined by setting a single $\kappa_i, i = t, g, b$ to zero.

Normally, MCFM identifies whether a process is $q\bar{q}$ - or gg -initiated, and running MCFM-RE in resummation mode does not lead to any problems. However, in cases like process 61, in fact WW production, MCFM includes in the NLO correction to a $q\bar{q}$ -initiated process formally higher-order gg -initiated contribution. As a consequence, not specifying the colour of the initial state leads to an ambiguity that is impossible to resolve. To avoid such problems, we have decided that, when running MCFM-RE in any resummation mode for ambiguous processes, the user must impose that a process is either $q\bar{q}$ - or gg -initiated, by making use of the MCFM flags `omitgg` and `ggonly`. Failure of doing so will result in MCFM-RE stopping and returning an error message.

B.2 Details of MCFM implementation

We modify MCFM version 8.0 to include the resummation of jet-veto effects. To this end there are two pieces that we must include, the computation of the luminosities $\mathcal{L}_{i.s.}^{(0)}, \mathcal{L}_{i.s.}^{(1)}$, and the Sudakov form factor combined with the functions $\mathcal{F}_{\text{clust}}, \mathcal{F}_{\text{correl}}$. The computation of the luminosities requires structural changes to MCFM whereas we are able to include the Sudakov form factor through an interface in `src/User/usercode.f90`.

The inclusion of the Sudakov form factor is the simplest change. The reweighting is included through the subroutine `userplotter`,

```
interface
  function sudakov(proc, M, muR, muF, Q, as, p, jet_radius, &
    &observable, small_r, small_r_R0, ptj_veto, order)
    ....
  end function
end interface
```

The user should not normally make changes to this function. The reweighting is applied to all histograms, including the default MCFM ones, as `wt` and `wt2` are `intent(inout)`, so our reweighting is applied globally. The cost of doing the reweighting here is that the cross section returned by the main MCFM program is wrong, or rather it includes only the contribution of the luminosities and not the Sudakov exponent. To that end we include the extra histogram `xsec`, a single-bin histogram to record the correct total cross section for runs with the jet-veto.

To include the luminosities we have to modify the factorisation scales of the PDFs. Instead of adding lots of switches to the default MCFM integration routines, we create our own special routines `resmNLL.f` (based on `lowint.f`) and `resmNNLL.f` (based on `virtint.f`), which we include in the `src/Procdep` directory along with the other default integration routines. The changes made in `resmNLL.f` are modest with respect to `lowint.f`, schematically

```
function resmNLL(r,wgt)
```

```

use rad_tools, only: Ltilde
implicit none
include 'types.f'
real(dp) :: resmNLLint

! resummation
include 'jetvtheto.f'
real(dp) :: facscaleLtilde
real(dp) :: L_tilde_arr(1)

L_tilde_arr = Ltilde((/ptj_veto/q_scale/), p_pow)
L_tilde = L_tilde_arr(1)
if (do_lumi) then
  facscaleLtilde = facscale*exp(-L_tilde)
else
  facscaleLtilde = facscale
end if

call fdist(ih1,xx(1),facscaleLtilde,fx1)
call fdist(ih2,xx(2),facscaleLtilde,fx2)

end

```

At the beginning of each event we determine \tilde{L} , and the modified `facscale` which we call `facscaleLtilde`. We then use this scale in the computation of the PDFs. The simplicity here is that at NLL accuracy all we need to do is change the factorisation scale and reweight, so these changes are very modest.

To perform the same calculation at NNLL is much more involved, since there are three separate actions that must be performed to compute the luminosity. First, we need to cast the virtual matrix element into the correct form for the resummation. We do this with a utility function in the file `src/Procdep/virtfin.f`, which performs the replacement detailed in eq. (A.14). This is carried out by the subroutine

```

subroutine virtfin(p,msq,msqv)
real(dp) :: p(mxpart, 4)
real(dp) :: msq(-nf:nf,-nf:nf), msqv(-nf:nf,-nf:nf)
end subroutine virtfin

```

where one must provide the array of momenta `p(mxpart,4)`, the tree level matrix element squared `msq(-nf:nf)` and the matrix element of the virtual corrections `msqv(-nf:nf)` (using the conventions of MCFM).

The second contribution to the luminosities comes from the convolution of the coefficient functions. To include this coefficient function we modify the integrated dipole functions located inside `src/Need/dipoles.f`, adding switches to choose between the different types of “dipoles” that we have added as well as the default MCFM subtraction dipole.

The third and final piece is performed in the new integration routine `src/Procdep/resmNNLL.f`. This calls the previous two routines, and then performs the convolutions of all coefficient functions with the PDFs.

```

function resmNNLL(r,wgt)
use rad_tools, only: Ltilde
implicit none
include 'types.f'
real(dp):: resmNNLLint

! resummation
include 'jetvheto.f'
real(dp) :: facscaleLtilde
real(dp) :: L_tilde_arr(1)

L_tilde_arr = Ltilde((/ptj_veto/q_scale/), p_pow)
L_tilde = L_tilde_arr(1)
if (do_lumi) then
  facscaleLtilde = facscale*exp(-L_tilde)
else
  facscaleLtilde = facscale
end if

!! Move contribution of collinear counterterm into the ‘‘dipoles’’
! AP(q,q,1)=+ason2pi*Cf*1.5_dp*epcorr
! AP(q,q,2)=+ason2pi*Cf*(-1._dp-z)*epcorr
! AP(q,q,3)=+ason2pi*Cf*2._dp/omz*epcorr
!! all AP terms are removed, those displayed here are just schematic

! extract the finite part of the virtual and modify for resummation
! must come before subtraction to get coefficient correct in checks
call virtfin(p, msq, msqv)

call fdist(ih1,xx(1),facscaleLtilde,fx1)
call fdist(ih2,xx(2),facscaleLtilde,fx2)
call fdist(ih1,x1onz,facscaleLtilde,fx1z)
call fdist(ih2,x2onz,facscaleLtilde,fx2z)

end

```

In addition, we can perform the matching with fixed-order using the same method we have used in computing the resummation. We modify the dipoles, this time to include the terms from the expansion of the resummation. With these one can then compute the matched distribution up to NNLL+NLO accuracy.

References

- [1] ATLAS collaboration, *Measurements of gluon-gluon fusion and vector-boson fusion*

- Higgs boson production cross-sections in the $H \rightarrow WW^* \rightarrow e\nu\mu\nu$ decay channel in pp collisions at $\sqrt{s} = 13$ TeV with the ATLAS detector*, *Phys. Lett.* **B789** (2019) 508 [[1808.09054](#)].
- [2] ATLAS collaboration, *Search for heavy resonances decaying into WW in the $e\nu\mu\nu$ final state in pp collisions at $\sqrt{s} = 13$ TeV with the ATLAS detector*, *Eur. Phys. J.* **C78** (2018) 24 [[1710.01123](#)].
- [3] ATLAS collaboration, *Measurement of the W^+W^- production cross section in pp collisions at a centre-of-mass energy of $\sqrt{s} = 13$ TeV with the ATLAS experiment*, *Phys. Lett.* **B773** (2017) 354 [[1702.04519](#)].
- [4] ATLAS collaboration, *Constraints on off-shell Higgs boson production and the Higgs boson total width in $ZZ \rightarrow 4\ell$ and $ZZ \rightarrow 2\ell 2\nu$ final states with the ATLAS detector*, *Phys. Lett.* **B786** (2018) 223 [[1808.01191](#)].
- [5] ATLAS collaboration, *Searches for heavy ZZ and ZW resonances in the $\ell\ell q\bar{q}$ and $\nu\nu q\bar{q}$ final states in pp collisions at $\sqrt{s} = 13$ TeV with the ATLAS detector*, *JHEP* **03** (2018) 009 [[1708.09638](#)].
- [6] ATLAS collaboration, *Search for diboson resonances with boson-tagged jets in pp collisions at $\sqrt{s} = 13$ TeV with the ATLAS detector*, *Phys. Lett.* **B777** (2018) 91 [[1708.04445](#)].
- [7] ATLAS collaboration, *Search for WW/WZ resonance production in $\ell\nu q\bar{q}$ final states in pp collisions at $\sqrt{s} = 13$ TeV with the ATLAS detector*, *JHEP* **03** (2018) 042 [[1710.07235](#)].
- [8] ATLAS collaboration, *Measurement of the four-lepton invariant mass spectrum in 13 TeV proton-proton collisions with the ATLAS detector*, [1902.05892](#).
- [9] CMS collaboration, *Measurements of the $pp \rightarrow ZZ$ production cross section and the $Z \rightarrow 4\ell$ branching fraction, and constraints on anomalous triple gauge couplings at $\sqrt{s} = 13$ TeV*, *Eur. Phys. J.* **C78** (2018) 165 [[1709.08601](#)].
- [10] CMS collaboration, *Measurements of properties of the Higgs boson decaying to a W boson pair in pp collisions at $\sqrt{s} = 13$ TeV*, *Phys. Lett.* **B791** (2019) 96 [[1806.05246](#)].
- [11] CMS collaboration, *Measurements of the Higgs boson width and anomalous HVV couplings from on-shell and off-shell production in the four-lepton final state*, [1901.00174](#).
- [12] E. W. N. Glover and J. J. van der Bij, *Vector Boson Pair Production via Gluon Fusion*, *Phys. Lett.* **B219** (1989) 488.
- [13] N. Kauer and G. Passarino, *Inadequacy of zero-width approximation for a light Higgs boson signal*, *JHEP* **08** (2012) 116 [[1206.4803](#)].
- [14] N. Kauer, *Interference effects for $H \rightarrow WW/ZZ \rightarrow \ell\bar{\nu}_\ell\bar{\ell}\nu_\ell$ searches in gluon fusion at the LHC*, *JHEP* **12** (2013) 082 [[1310.7011](#)].

- [15] F. Caola and K. Melnikov, *Constraining the Higgs boson width with ZZ production at the LHC*, *Phys. Rev.* **D88** (2013) 054024 [[1307.4935](#)].
- [16] W. Buchmuller and D. Wyler, *Effective Lagrangian Analysis of New Interactions and Flavor Conservation*, *Nucl. Phys.* **B268** (1986) 621.
- [17] B. Grzadkowski, M. Iskrzynski, M. Misiak and J. Rosiek, *Dimension-Six Terms in the Standard Model Lagrangian*, *JHEP* **10** (2010) 085 [[1008.4884](#)].
- [18] G. F. Giudice, C. Grojean, A. Pomarol and R. Rattazzi, *The Strongly-Interacting Light Higgs*, *JHEP* **06** (2007) 045 [[hep-ph/0703164](#)].
- [19] J. Elias-Miro, J. R. Espinosa, E. Masso and A. Pomarol, *Higgs windows to new physics through $d=6$ operators: constraints and one-loop anomalous dimensions*, *JHEP* **11** (2013) 066 [[1308.1879](#)].
- [20] R. V. Harlander and T. Neumann, *Probing the nature of the Higgs-gluon coupling*, *Phys. Rev.* **D88** (2013) 074015 [[1308.2225](#)].
- [21] J. Ellis, C. W. Murphy, V. Sanz and T. You, *Updated Global SMEFT Fit to Higgs, Diboson and Electroweak Data*, *JHEP* **06** (2018) 146 [[1803.03252](#)].
- [22] A. Azatov, C. Grojean, A. Paul and E. Salvioni, *Taming the off-shell Higgs boson*, *Zh. Eksp. Teor. Fiz.* **147** (2015) 410 [[1406.6338](#)].
- [23] M. Buschmann, D. Goncalves, S. Kuttimalai, M. Schonherr, F. Krauss and T. Plehn, *Mass Effects in the Higgs-Gluon Coupling: Boosted vs Off-Shell Production*, *JHEP* **02** (2015) 038 [[1410.5806](#)].
- [24] ATLAS collaboration, *Measurement of W^+W^- production in pp collisions at $\sqrt{s} = 7$ TeV with the ATLAS detector and limits on anomalous WWZ and $WW\gamma$ couplings*, *Phys. Rev.* **D87** (2013) 112001 [[1210.2979](#)].
- [25] CMS collaboration, *Measurement of the W^+W^- Cross Section in pp Collisions at $\sqrt{s} = 7$ TeV and Limits on Anomalous $WW\gamma$ and WWZ Couplings*, *Eur. Phys. J.* **C73** (2013) 2610 [[1306.1126](#)].
- [26] CMS collaboration, *Measurement of W^+W^- and ZZ Production Cross Sections in pp Collisions at $\sqrt{s} = 8$ TeV*, *Phys. Lett.* **B721** (2013) 190 [[1301.4698](#)].
- [27] P. Jaiswal and T. Okui, *Explanation of the WW excess at the LHC by jet-veto resummation*, *Phys. Rev.* **D90** (2014) 073009 [[1407.4537](#)].
- [28] P. F. Monni and G. Zanderighi, *On the excess in the inclusive $W^+W^- \rightarrow l^+l^-\nu\bar{\nu}$ cross section*, *JHEP* **05** (2015) 013 [[1410.4745](#)].
- [29] T. Becher, R. Frederix, M. Neubert and L. Rothen, *Automated NNLL + NLO resummation for jet-veto cross sections*, *Eur. Phys. J.* **C75** (2015) 154 [[1412.8408](#)].
- [30] E. Re, M. Wiesemann and G. Zanderighi, *NNLOPS accurate predictions for W^+W^- production*, *JHEP* **12** (2018) 121 [[1805.09857](#)].
- [31] P. Jaiswal, P. Meade and H. Ramani, *Precision diboson measurements and the*

- interplay of p_T and jet-veto resummations*, *Phys. Rev.* **D93** (2016) 093007 [[1509.07118](#)].
- [32] J. Bellm, S. Gieseke, N. Greiner, G. Heinrich, S. Plätzer, C. Reuschle et al., *Anomalous coupling, top-mass and parton-shower effects in W^+W^- production*, *JHEP* **05** (2016) 106 [[1602.05141](#)].
- [33] I. Moult and I. W. Stewart, *Jet Vetoes interfering with $H \rightarrow WW$* , *JHEP* **09** (2014) 129 [[1405.5534](#)].
- [34] A. Banfi, G. P. Salam and G. Zanderighi, *Principles of general final-state resummation and automated implementation*, *JHEP* **03** (2005) 073 [[hep-ph/0407286](#)].
- [35] ATLAS collaboration, *Measurement of the transverse momentum and ϕ_η^* distributions of Drell–Yan lepton pairs in proton–proton collisions at $\sqrt{s} = 8$ TeV with the ATLAS detector*, *Eur. Phys. J.* **C76** (2016) 291 [[1512.02192](#)].
- [36] A. Banfi, P. F. Monni, G. P. Salam and G. Zanderighi, *Higgs and Z-boson production with a jet veto*, *Phys. Rev. Lett.* **109** (2012) 202001 [[1206.4998](#)].
- [37] T. Becher, M. Neubert and L. Rothen, *Factorization and N^3LL_p+NNLO predictions for the Higgs cross section with a jet veto*, *JHEP* **10** (2013) 125 [[1307.0025](#)].
- [38] I. W. Stewart, F. J. Tackmann, J. R. Walsh and S. Zuberi, *Jet p_T resummation in Higgs production at $NNLL' + NNLO$* , *Phys. Rev.* **D89** (2014) 054001 [[1307.1808](#)].
- [39] <https://jetvheto.hepforge.org/>.
- [40] B. Fuks and R. Ruiz, *A comprehensive framework for studying W' and Z' bosons at hadron colliders with automated jet veto resummation*, *JHEP* **05** (2017) 032 [[1701.05263](#)].
- [41] M. Cacciari, G. P. Salam and G. Soyez, *The anti- k_t jet clustering algorithm*, *JHEP* **04** (2008) 063 [[0802.1189](#)].
- [42] A. Banfi, G. P. Salam and G. Zanderighi, *$NLL+NNLO$ predictions for jet-veto efficiencies in Higgs-boson and Drell-Yan production*, *JHEP* **06** (2012) 159 [[1203.5773](#)].
- [43] S. Catani and M. Grazzini, *QCD transverse-momentum resummation in gluon fusion processes*, *Nucl. Phys.* **B845** (2011) 297 [[1011.3918](#)].
- [44] <https://mcfm.fnal.gov/>.
- [45] ATLAS collaboration, *Measurement of the W^+W^- production cross section in proton-proton collisions at $\sqrt{s} = 8$ TeV with the ATLAS detector*, .
- [46] J. M. Campbell and F. Tramontano, *Next-to-leading order corrections to Wt production and decay*, *Nucl. Phys.* **B726** (2005) 109 [[hep-ph/0506289](#)].
- [47] J. Butterworth et al., *PDF4LHC recommendations for LHC Run II*, *J. Phys.* **G43** (2016) 023001 [[1510.03865](#)].

- [48] A. Buckley, J. Ferrando, S. Lloyd, K. Nordström, B. Page, M. Rüfenacht et al., *LHAPDF6: parton density access in the LHC precision era*, *Eur. Phys. J.* **C75** (2015) 132 [[1412.7420](#)].
- [49] LHC HIGGS CROSS SECTION WORKING GROUP collaboration, *Handbook of LHC Higgs Cross Sections: 1. Inclusive Observables*, [1101.0593](#).
- [50] A. Banfi, F. Caola, F. A. Dreyer, P. F. Monni, G. P. Salam, G. Zanderighi et al., *Jet-vetoed Higgs cross section in gluon fusion at $N^3LO+NNLL$ with small- R resummation*, *JHEP* **04** (2016) 049 [[1511.02886](#)].
- [51] R. Boughezal, X. Liu, F. Petriello, F. J. Tackmann and J. R. Walsh, *Combining Resummed Higgs Predictions Across Jet Bins*, *Phys. Rev.* **D89** (2014) 074044 [[1312.4535](#)].
- [52] C. Grojean, E. Salvioni, M. Schlaffer and A. Weiler, *Very boosted Higgs in gluon fusion*, *JHEP* **05** (2014) 022 [[1312.3317](#)].
- [53] ATLAS collaboration, *Search for the Standard Model Higgs boson in the $H \rightarrow WW^{(*)} \rightarrow l\nu l\nu$ decay mode with 4.7 fb of ATLAS data at $\sqrt{s} = 7$ TeV*, *Phys. Lett.* **B716** (2012) 62 [[1206.0756](#)].
- [54] CMS collaboration, *Search for the standard model Higgs boson decaying to W^+W^- in the fully leptonic final state in pp collisions at $\sqrt{s} = 7$ TeV*, *Phys. Lett.* **B710** (2012) 91 [[1202.1489](#)].
- [55] D. L. Rainwater and D. Zeppenfeld, *Observing $H \rightarrow W^*W^* \rightarrow e^\pm\mu^\mp \cancel{p}_T$ in weak boson fusion with dual forward jet tagging at the CERN LHC*, *Phys. Rev.* **D60** (1999) 113004 [[hep-ph/9906218](#)].
- [56] S. Alioli, P. Nason, C. Oleari and E. Re, *A general framework for implementing NLO calculations in shower Monte Carlo programs: the POWHEG BOX*, *JHEP* **06** (2010) 043 [[1002.2581](#)].
- [57] S. Frixione, P. Nason and C. Oleari, *Matching NLO QCD computations with Parton Shower simulations: the POWHEG method*, *JHEP* **11** (2007) 070 [[0709.2092](#)].
- [58] P. Nason, *A New method for combining NLO QCD with shower Monte Carlo algorithms*, *JHEP* **11** (2004) 040 [[hep-ph/0409146](#)].
- [59] P. Nason and G. Zanderighi, *W^+W^- , WZ and ZZ production in the POWHEG-BOX-V2*, *Eur. Phys. J.* **C74** (2014) 2702 [[1311.1365](#)].
- [60] T. Sjöstrand, S. Ask, J. R. Christiansen, R. Corke, N. Desai, P. Ilten et al., *An Introduction to PYTHIA 8.2*, *Comput. Phys. Commun.* **191** (2015) 159 [[1410.3012](#)].
- [61] J. Alwall, R. Frederix, S. Frixione, V. Hirschi, F. Maltoni, O. Mattelaer et al., *The automated computation of tree-level and next-to-leading order differential cross sections, and their matching to parton shower simulations*, *JHEP* **07** (2014) 079 [[1405.0301](#)].
- [62] S. Frixione, F. Stoeckli, P. Torrielli and B. R. Webber, *NLO QCD corrections in Herwig++ with MC@NLO*, *JHEP* **01** (2011) 053 [[1010.0568](#)].

- [63] S. Frixione and B. R. Webber, *Matching NLO QCD computations and parton shower simulations*, *JHEP* **06** (2002) 029 [[hep-ph/0204244](#)].
- [64] S. Frixione, *A General approach to jet cross-sections in QCD*, *Nucl. Phys.* **B507** (1997) 295 [[hep-ph/9706545](#)].
- [65] S. Frixione, Z. Kunszt and A. Signer, *Three jet cross-sections to next-to-leading order*, *Nucl. Phys.* **B467** (1996) 399 [[hep-ph/9512328](#)].
- [66] M. Bahr et al., *Herwig++ Physics and Manual*, *Eur. Phys. J.* **C58** (2008) 639 [[0803.0883](#)].
- [67] J. Bellm et al., *Herwig 7.0/Herwig++ 3.0 release note*, *Eur. Phys. J.* **C76** (2016) 196 [[1512.01178](#)].
- [68] H.-L. Lai, M. Guzzi, J. Huston, Z. Li, P. M. Nadolsky, J. Pumplin et al., *New parton distributions for collider physics*, *Phys. Rev.* **D82** (2010) 074024 [[1007.2241](#)].
- [69] J. Pumplin, D. R. Stump, J. Huston, H. L. Lai, P. M. Nadolsky and W. K. Tung, *New generation of parton distributions with uncertainties from global QCD analysis*, *JHEP* **07** (2002) 012 [[hep-ph/0201195](#)].
- [70] A. Banfi, G. P. Salam and G. Zanderighi, *Resummed event shapes at hadron - hadron colliders*, *JHEP* **08** (2004) 062 [[hep-ph/0407287](#)].
- [71] M. Dasgupta and G. P. Salam, *Resummation of nonglobal QCD observables*, *Phys. Lett.* **B512** (2001) 323 [[hep-ph/0104277](#)].
- [72] J. K. L. Michel, P. Pietrulewicz and F. J. Tackmann, *Jet Veto Resummation with Jet Rapidity Cuts*, *JHEP* **04** (2019) 142 [[1810.12911](#)].
- [73] T. Gehrmann, M. Grazzini, S. Kallweit, P. Maierhöfer, A. von Manteuffel, S. Pozzorini et al., *W^+W^- Production at Hadron Colliders in Next to Next to Leading Order QCD*, *Phys. Rev. Lett.* **113** (2014) 212001 [[1408.5243](#)].
- [74] F. Cascioli, T. Gehrmann, M. Grazzini, S. Kallweit, P. Maierhöfer, A. von Manteuffel et al., *ZZ production at hadron colliders in NNLO QCD*, *Phys. Lett.* **B735** (2014) 311 [[1405.2219](#)].
- [75] F. Caola, J. M. Henn, K. Melnikov, A. V. Smirnov and V. A. Smirnov, *Two-loop helicity amplitudes for the production of two off-shell electroweak bosons in gluon fusion*, *JHEP* **06** (2015) 129 [[1503.08759](#)].
- [76] A. von Manteuffel and L. Tancredi, *The two-loop helicity amplitudes for $gg \rightarrow V_1 V_2 \rightarrow 4$ leptons*, *JHEP* **06** (2015) 197 [[1503.08835](#)].
- [77] F. Caola, K. Melnikov, R. Rötsch and L. Tancredi, *QCD corrections to ZZ production in gluon fusion at the LHC*, *Phys. Rev.* **D92** (2015) 094028 [[1509.06734](#)].
- [78] F. Caola, K. Melnikov, R. Rötsch and L. Tancredi, *QCD corrections to W^+W^- production through gluon fusion*, *Phys. Lett.* **B754** (2016) 275 [[1511.08617](#)].
- [79] F. Caola, M. Dowling, K. Melnikov, R. Rötsch and L. Tancredi, *QCD corrections*

- to vector boson pair production in gluon fusion including interference effects with off-shell Higgs at the LHC, *JHEP* **07** (2016) 087 [[1605.04610](#)].
- [80] J. M. Campbell, R. K. Ellis, M. Czakon and S. Kirchner, *Two loop correction to interference in $gg \rightarrow ZZ$* , *JHEP* **08** (2016) 011 [[1605.01380](#)].
- [81] M. Grazzini, S. Kallweit, M. Wiesemann and J. Y. Yook, *ZZ production at the LHC: NLO QCD corrections to the loop-induced gluon fusion channel*, *JHEP* **03** (2019) 070 [[1811.09593](#)].
- [82] M. Grazzini, S. Kallweit and D. Rathlev, *ZZ production at the LHC: fiducial cross sections and distributions in NNLO QCD*, *Phys. Lett.* **B750** (2015) 407 [[1507.06257](#)].
- [83] S. Kallweit and M. Wiesemann, *ZZ production at the LHC: NNLO predictions for $2\ell 2\nu$ and 4ℓ signatures*, *Phys. Lett.* **B786** (2018) 382 [[1806.05941](#)].
- [84] M. Grazzini, S. Kallweit, S. Pozzorini, D. Rathlev and M. Wiesemann, *W^+W^- production at the LHC: fiducial cross sections and distributions in NNLO QCD*, *JHEP* **08** (2016) 140 [[1605.02716](#)].
- [85] M. Grazzini, S. Kallweit and M. Wiesemann, *Fully differential NNLO computations with MATRIX*, *Eur. Phys. J.* **C78** (2018) 537 [[1711.06631](#)].
- [86] M. Grazzini, S. Kallweit, D. Rathlev and M. Wiesemann, *$W^\pm Z$ production at hadron colliders in NNLO QCD*, *Phys. Lett.* **B761** (2016) 179 [[1604.08576](#)].
- [87] M. Grazzini, S. Kallweit, D. Rathlev and M. Wiesemann, *$W^\pm Z$ production at the LHC: fiducial cross sections and distributions in NNLO QCD*, *JHEP* **05** (2017) 139 [[1703.09065](#)].
- [88] CMS collaboration, *Measurement of differential and integrated fiducial cross sections for Higgs boson production in the four-lepton decay channel in pp collisions at $\sqrt{s} = 7$ and 8 TeV*, *JHEP* **04** (2016) 005 [[1512.08377](#)].
- [89] PARTICLE DATA GROUP collaboration, *Review of Particle Physics*, *Phys. Rev.* **D98** (2018) 030001.
- [90] A. Hocker, H. Lacker, S. Laplace and F. Le Diberder, *A New approach to a global fit of the CKM matrix*, *Eur. Phys. J.* **C21** (2001) 225 [[hep-ph/0104062](#)].
- [91] G. Cowan, K. Cranmer, E. Gross and O. Vitells, *Asymptotic formulae for likelihood-based tests of new physics*, *Eur. Phys. J.* **C71** (2011) 1554 [[1007.1727](#)].
- [92] ATLAS collaboration, *Combined measurements of Higgs boson production and decay using up to 80 fb^{-1} of proton–proton collision data at $\sqrt{s} = 13 \text{ TeV}$ collected with the ATLAS experiment*, .
- [93] S. Pascoli, R. Ruiz and C. Weiland, *Safe Jet Vetoes*, *Phys. Lett.* **B786** (2018) 106 [[1805.09335](#)].
- [94] S. Pascoli, R. Ruiz and C. Weiland, *Heavy neutrinos with dynamic jet vetoes*:

*multilepton searches at $\sqrt{s} = 14, 27, \text{ and } 100 \text{ TeV}$, [JHEP 06 \(2019\) 049](#)
[1812.08750].*

- [95] J. M. Campbell and R. K. Ellis, *Radiative corrections to $Z b \text{ anti-}b$ production*, [Phys. Rev. D62 \(2000\) 114012](#) [[hep-ph/0006304](#)].